Solvent Effect on Morphological, Crystalline and Electronic Properties of Triple-Cation Lead-Tin Double-Halide Perovskite Thin Films and Their Air Stability

Yi- Yu Lin

A thesis

submitted in partial fulfillment of the

requirements for the degree of

Master of Science

University of Washington

2018

Reading Committee:

Qiuming Yu, Chair

Samson Jenekhe

Program Authorized to Offer Degree:

Chemical Engineering

Abstract

Solvent Effect on Morphological, Crystalline and Electronic Properties of Triple-Cation Lead-Tin Double-Halide Perovskite Thin Films and Their Air Stability

Yi- Yu Lin

Chair of the Supervisory Committee:
Professor Qiuming Yu
Department of Chemical Engineering

Recently, triple cation Cs/MA/FA and mixed halide Br/I lead perovskites were found to improve the stability and efficiency of perovskite solar cells. However, the replacement of Pb with Sn has not been fully developed. In this work, we focused on the investigation of the solvent effect on morphological, crystalline and electronic properties of the perovskite thin films with the compositions of $Cs_x(MA_{0.17}FA_{0.83})_{1-x}Pb_{1-y}Sn_y(I_{0.83}Br_{0.17})_3$, where x = 0.05, 0.1, and 0.2 and y = 0, 0.25, 0.50 0.75, and 1.0. By optimizing the mixed solvents in making perovskite precursor solutions, anti-solvent volumes in wash step and annealing temperature, as well as adding anti-oxidation agent, we were able to fabricate pinhole-free perovskite thin films with shiny, uniform dark- color. The surface morphology, crystal structure and optical band gap were investigated using scanning electron microscope (SEM), X-Ray diffraction (XRD), and UV-Vis absorption spectroscopy. The air stability of the perovskite thin films was also assessed by acquiring SEM images and XRD patterns after the films were stored in an ambient condition for 10 days. Phase segregation occurred as shown in XRD peak shifts and white rods around grain boundaries in SEM images, which contain high Sn, Br, and F elements.

Table of Contents

List of Figures

ACKNOWLEDGEMENTS

I would express my sincere appreciation to my advisor Professor Qiuming Yu for her guidance and encouragement, to the group members David Galvan, Monica Esopi, Gabriella Tosado, Erjin Zheng, Xiaoyu Zhang, Vidit Parekh, Zhiyin Niu, Hao Dong, Chen Cai and E-Lin Liu for their ideas, and to my parents for their invaluable support. I would acknowledge the Molecular Analysis Facility, a National Nanotechnology Coordinated Infrastructure site at the University of Washington which is supported in part by the National Science Foundation (grant ECC-1542101), the University of Washington, the Molecular Engineering & Sciences Institute, the Clean Energy Institute, and the National Institutes of Health for access the necessary characterization tools. I would also like to thank Ryan Stoddard in Professor Hugh Hillhouse lab for photoluminescence measurements.

Chapter 1 – INTRODUCTION

Hybrid organic- inorganic metal halide perovskite solar cells attracted attention with their high power conversion efficiency (PCE). A record PCE have reached over 22 % [1 -6, 7]. The perovskite structure is ABX_3, where A is the organic or inorganic cation, such as methylammonium (MA^+), formamidinium (FA^+), and cesium (Cs^+) [8, 9, 10]; B is the metal cation, such as lead (Pb^{2+}) and tin (Sn^{2+}) [8]; X is the halide anion, such as iodide (I^-), bromide (Br^-) and chloride (Cl^-) [1, 3, 8-10, 11, 12, 13]. The high performance is attributed to the material properties such as the high absorption of visible to near infrared light with a sharp band edge and tunable bandgap [4].

Methylammonium lead triiodide ($MAPbI_3$) perovskites cannot reach a PCE over 20 %, and it faces several complex challenges such as thermal and moisture instability [4, 8, 14-17]. Quick degradation was observed when they are exposed to moisture and long-time illumination [5]. Formamidinium lead triiodide ($FAPbI_3$) perovskites have the advantage of the reduction in bandgap to 1.48 eV, which allows higher solar light conversion efficiency, and the expansion of perovskite lattice because of the larger size of formamidinium than methylammonium. However, $FAPbI_3$ is lack of structure stability. The yellow impure δ -phase accompanies the black α -phase at room temperature [2, 4, 18, 26, 28- 30]. The inorganic perovskite Cesium lead triiodide ($CsPbI_3$) is suitable for improving thermal stability since Cs cation is less volatile, but it also suffers from the impure δ -phase at room temperature and is only stable at temperatures above 300℃ [2, 24]. Since pure perovskites encounter thermal or structural instabilities, the importance of mix cations and halides come into mind to achieve thermal and structural stability. Saliba *et al.* used a triple Cs/MA/FA cation mixture where small quantity of Cs was added to effectively

suppress the yellow δ-phase, demonstrated a PCE over 21 % and retained PCE of 18 % after 250 hours in nitrogen glove box at room temperature under constant illumination [2].

To reduce environmental toxicity yet not affect the photovoltaic performance, replacing lead with tin was explored [16, 19]. The main reason is both lead and tin belong to 14 metal group in the periodic table and have similar ionic radii (Pb^{2+} 1.19 Å and Sn^{2+} 1.15 Å), which would have minimum effect on the lattice parameters. The Sn-based perovskites had a reported narrower bandgap of 1.2~ 1.3 eV, which can absorb broader solar light, leading to higher PCE [2, 20]. However, with Sn substitution especially over 25 % Sn, poorer perovskite film morphology and coverage were observed due to the rapid crystallization during spin-coating, resulting in poor device performance [19]. In addition, the oxidation of Sn^{2+} to Sn^{4+} degrades the perovskites due to the weak inert pair effect of Sn comparing to Pb [19, 21].

In this work, based on the formula of Cs/FA/MA triple cation with mixed halides of I/Br [4], we introduced Sn to form Pb-Sn alloyed and even pure Sn perovskites to reduce the environmental toxicity while keeping the stability of perovskite solar cells. We fabricated perovskite thin films with the compositions of $Cs_x(MA_{0.17}FA_{0.83})_{1-x}Pb_{1-y}Sn_y(I_{0.83}Br_{0.17})_3$ with x = 0.05, 0.10, and 0.20 and y = 0, 0.25, 0.50, 0.75, and 1.0. We optimized the mixed solvents for precursor solutions, anti-solvent volume for washing and annealing temperature. We focused on the analysis of perovskite thin films with X -Ray Diffraction (XRD) to obtain the crystal properties, UV-Vis and photoluminescence (PL) spectroscopy to estimate the bandgaps, and scanning electron microscope (SEM) to gain surface morphologies. To study the stability of the perovskite thin films, the films were left in ambient condition after initial analysis. Slight XRD peak shifts and white segregates in SEM images were observed after 10 days in ambient condition.

Chapter 2 – EXPERIMENTAL METHODS

2.1 Materials

Lead (II) iodide (PbI_2, 99 %), tin (II) iodide (SnI_2, 99.99 %) , lead (II) bromide ($PbBr_2$, 99.999 %), cesium iodide (CsI, 99.999 %), tin (II) fluoride (SnF_2 99 %), , chlorobenzene (anhydrous, 99.8 %), toluene (anhydrous, 99.8 %), ɣ-butyrolactone (GBL, ≥ 99 %), N,N-dimethyl sulfoxide (DMSO, anhydrous, ≥ 99.9 %), and N,N- dimethylformamide (DMF, anhydrous, 99.8 %) were purchased from Sigma-Aldrich (St. Louis, Missouri) without further purification. Methylammonium iodide (MAI), formamidinium iodide (FAI), and formamidinium bromide (FABr) were purchased from Greatcell Solar (Queanbeyan, Australia) without further purification.

2.2 Perovskite Thin Films Fabrication

Plain glass was cut into 15 mm x 15 mm substrates, then were cleaned via ultrasonication for 15 min in detergent in Millipore deionized water, Millipore deionized water, acetone, and isopropanol in sequence. The substrates were treated with oxygen plasma under 100 W for 10 min.

2.2.1 Mixed Solvent of GBL and DMSO with Toluene Anti-Solvent

The perovskite precursor solutions were made by dissolving MAI, FAI, PbI_2, $PbBr_2$, SnI_2, and FABr, at the corresponding molar ratios in GBL and DMSO (volume ratio 7:3) with a total concentration of 1 M and 2.5 M. A 10% SnF_2 per molar weight of SnI_2 was added in the precursor solution as a reducing agent, some of the fabrication were mixed without SnF_2. The precursors were mixed at 60 °C for 1 h. CsI was dissolved in DMSO at a concentration of 1.5 M and added to the precursor to achieve the correct triple cation composition. A 70 µL drop of precursor solution was spin-coated on a cleaned glass substrate at 500 rpm for 5 s, 1000 rpm for

15 s, and 4000 rpm for 40 s in a nitrogen glove box. A toluene anti-solvent was *in situ* dripped onto the substrate during the last 15 s of the third spin-coating step. The volume of the anti-solvent was 700 µL, 700 µL, 600 µL, 500 µL, and 500 µL for $Cs_x(MA_{0.17}FA_{0.83})_{1-x}Pb_{1-y}Sn_y(I_{0.83}Br_{0.17})_3$ perovskites with y = 0, 0.25, 0.5, 0.75 and 1.0, respectively. The perovskite films were then thermally annealed at 100 °C for 10 min, except for $Cs_{0.1}(MA_{0.17}FA_{0.83})_{0.9}Sn(I_{0.83}Br_{0.17})_3$ and $Cs_{0.2}(MA_{0.17}FA_{0.83})_{0.8}Sn(I_{0.83}Br_{0.17})_3$ which were thermally annealed at 110 °C for 10 min.

2.2.2 Mixed Solvent of DMF and DMSO with Chlorobenzene Anti-Solvent

The perovskite precursor solutions were made by dissolving MAI, FAI, PbI_2, $PbBr_2$ and SnI_2 at the corresponding molar ratios in DMF and DMSO (volume ratio 4:1) with a total concentration of 1 M and 2.5 M. The precursors were mixed at 60 °C for 1 h. CsI was dissolved in DMSO at a concentration of 1.5 M and added to the precursor to achieve the correct triple cation composition. A 70 µL drop of precursor solution was spin-coated on a cleaned glass substrate at 1000 rpm for 10 s and 6000 rpm for 20 s in a nitrogen glove box. A 100 µL chlorobenzene anti-solvent was *in situ* dripped onto the substrate during the last 5 s of the second spin-coating step. The perovskite films were then thermally annealed at 100 °C for 1 hr.

2.2.3 Mixed Solvent of DMF and DMSO with Toluene Anti-Solvent

The perovskite precursor solutions were made by dissolving MAI, FAI, PbI_2, $PbBr_2$ and SnI_2 at the corresponding molar ratios in DMF and DMSO (volume ratio 4:1) with a total concentration of 1 M and 2.5 M. The precursors were mixed at 60 °C for 1 h. CsI was dissolved in DMSO at a concentration of 1.5 M and added to the precursor to achieve the correct triple cation composition. A 70 µL drop of precursor solution was spin-coated on a cleaned glass substrate at 1000 rpm for 15 s and 4000 rpm for 45 s in a nitrogen glove box. A 700 µL toluene

anti-solvent was *in situ* dripped onto the substrate during the last 15 s of the second spin-coating step. The perovskite films were then thermally annealed at 100 °C for 10 min.

2.3 Perovskite Thin Films Characterization

Scanning electron microscopy (SEM) and energy dispersion spectroscopy (EDS) were acquired using FEI Sirion SEM operated at 5 kV and 15 kV to gain surface morphology and elemental compositions of perovskite thin films, respectively. Two-dimensional X-Ray diffraction (XRD) patterns were collected with Bruker D8 Discover Microfocus diffractometer using Cu Kα radiation (λ = 1.5419 Å) to investigate crystalline structures of perovskite thin films. Atomic Force Microscopy (AFM) images were collected with a Bruker/Veeco/DI Multimode AFM-2. Ultraviolet-visible (UV-Vis) absorption spectra were collected using a Varian Cary 5000 UV-Vis-NIR spectrophotometer. Photoluminescence (PL) spectra were obtained with a modified Horiba LabRAM HR-800 with 532 nm laser excitation and a Czerny−Turner monochromator blazed at 1200 nm. Measurements were conducted at 1 Sun above bandgap equivalent photon flux with a 532 nm cw laser. The PL experiments were conducted in a N_2-filled KF flange with a borosilicate glass window.

2.4 Air stability tests

All perovskite thin films were left in ambient condition for 10 days after initial analysis. The SEM images were acquired to gain surface morphologies and the XRD patterns were collected to investigate crystalline structures of air exposed perovskite thin films.

Chapter 3 – RESULTS AND DISSCUSSION

3.1 Perovskite Thin Films Fabricated with GBL: DMSO Mixed Solvent and Toluene Anti-Solvent

To achieve uniform, dark color perovskite films, we used a one-step anti-solvent method. Reported in literature, the method involved GBL: DMSO for the precursor solutions, and toluene as the anti-solvent for washing [21]. To make description simple, we will use the notation Cs_xSn_y to represent the thin films. For example, $Cs_{0.05}Sn_{0.1}$ represents the thin films with the composition of $Cs_{0.05}(MA_{0.17}FA_{0.83})_{0.95}Pb_{0.9}Sn_{0.1}(I_{0.83}Br_{0.17})_3$.

3.1.1 $Cs_x(MA_{0.17}FA_{0.83})_{1-x}Pb_{1-y}Sn_y(I_{0.83}Br_{0.17})_3$ Perovskite Thin Films Fabricated with the Addition of SnF_2

Some of the results presented in this section were included in the manuscript to be submitted to Advanced Energy Materials by Gabriella Tosado, Yi-Yu Lin, Erjin Zheng, and Qiuming Yu*, with the title “Impact of Cesium in Phase and Device Stability of Triple Cation Pb-Sn Mixed-Halide Perovskite Solar Cells”.

All precursors (MAI, FAI, PbI_2, $PbBr_2$ and SnI_2) were dissolved in a DMSO: GBL (3:7, v/v) co-solvent solution to a total concentration of 1 M and 2.5 M. We also added 10% mol SnF_2 with respect to Sn content to suppress formation of Sn^{4+} [8, 11, 22, 23]. The thin film was spin coated on a cleaned glass substrate at 500 rpm for 5 s, 1000 rpm for 15 s, and 4000 rpm for 40 s with a 700 µL toluene anti-solvent dropped during the last 15 s of the second spin coating step.

With a total concentration of 1 M, the perovskite thin films are more transparent with lighter brown color as shown in Table 1. The SEM images (Figure 3.1) show dense and uniform grains even though light color. The white grains shown in the SEM images of two films containing 10% Cs were suspected to be the segregated or undissolved SnF_2 [8, 11, 22, 23], since

a 10% mol SnF_2 with respect to Sn content was added to the precursor solution to suppress formation of Sn^{4+}. The thickness of these perovskite films was around 200-300 nm estimated from the cross-section SEM images in Figures 3.2 (a) and (b). Because the films were thin, XRD signals were weak with more noise (Figure 3.3). For example, the (110) plane peak even did not show for $Cs_{0.1}Sn_{0.25}$ film. Although the thin films had light brown semi- transparent color, the UV- Vis absorption spectra still showed the absorption edges between 800 ~ 900 nm.

Table 1. The photographs of the $Cs_x(MA_{0.17}FA_{0.83})_{1-x}Pb_{1-y}Sn_y(I_{0.83}Br_{0.17})_3$ perovskite thin films taken right after annealing. All the films were fabricated using a total precursor concentration of 1M and 700 µL toluene anti-solvent.

	$Sn_{0.25}$	$Sn_{0.5}$
$Cs_{0.1}$		
$Cs_{0.2}$		

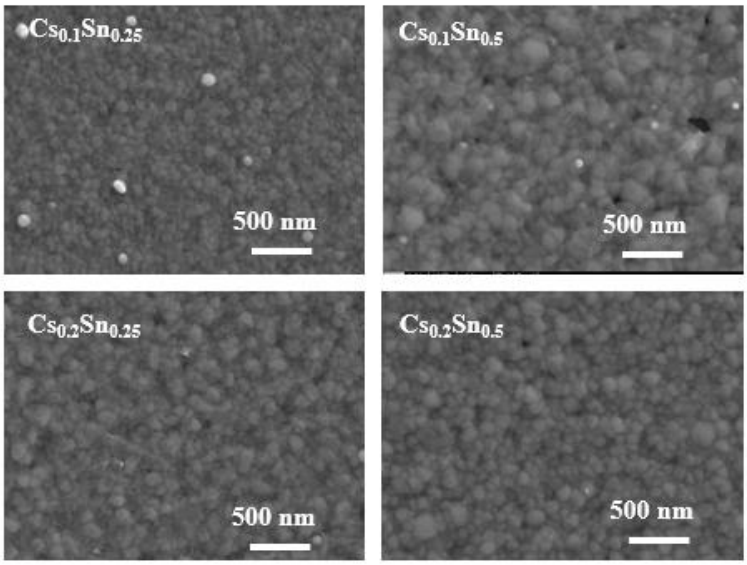

Figure 3. 1. SEM images of $Cs_x(MA_{0.17}FA_{0.83})_{1-x}Pb_{1-y}Sn_y(I_{0.83}Br_{0.17})_3$ perovskite thin films with x = 0.1 and 0.2 and y = 0.25 and 0.5, fabricated using a total precursor concentration of 1 M and 700 µL toluene anti-solvent.

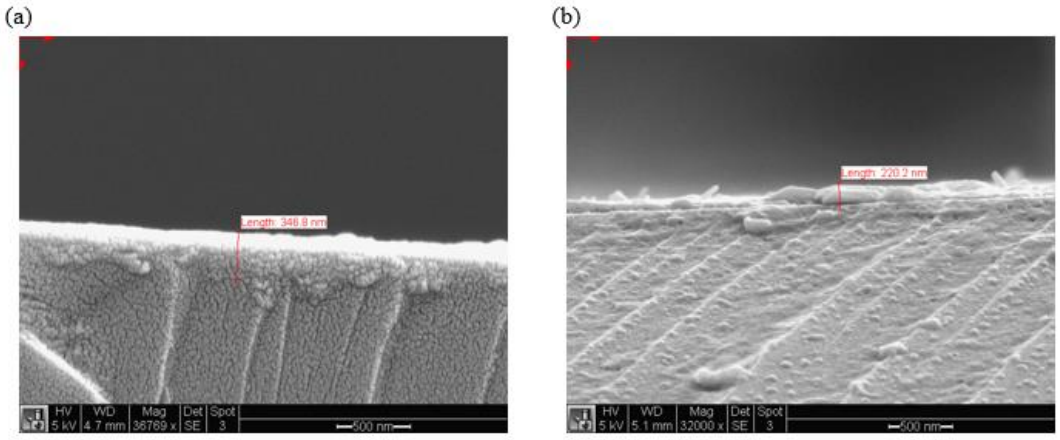

Figure 3. 2. SEM cross-section images of $Cs_x(MA_{0.17}FA_{0.83})_{1-x}Pb_{1-y}Sn_y(I_{0.83}Br_{0.17})_3$ perovskite thin films with (a) x = 0.1, y = 0.25 and (b) x = 0.2, y = 0.5 with 700 µL toluene anti-solvent with a total concentration of 1 M.

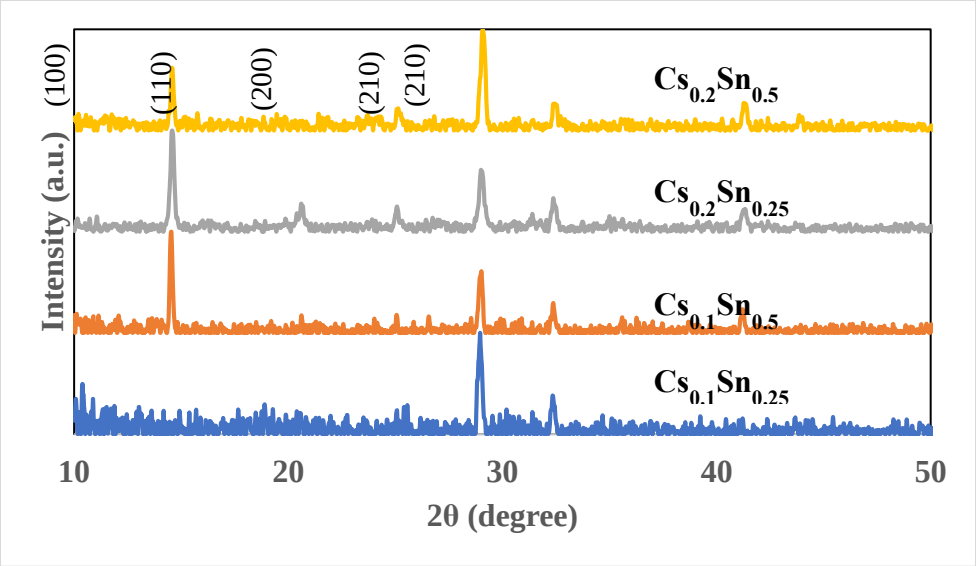

Figure 3. 3. X-Ray Diffraction patterns of $Cs_x(MA_{0.17}FA_{0.83})_{1-x}Pb_{1-y}Sn_y(I_{0.83}Br_{0.17})_3$ perovskite thin films with x = 0.1 and 0.2 and y = 0.25 and 0.5 with 700 µL toluene anti-solvent and a total concentration of 1 M.

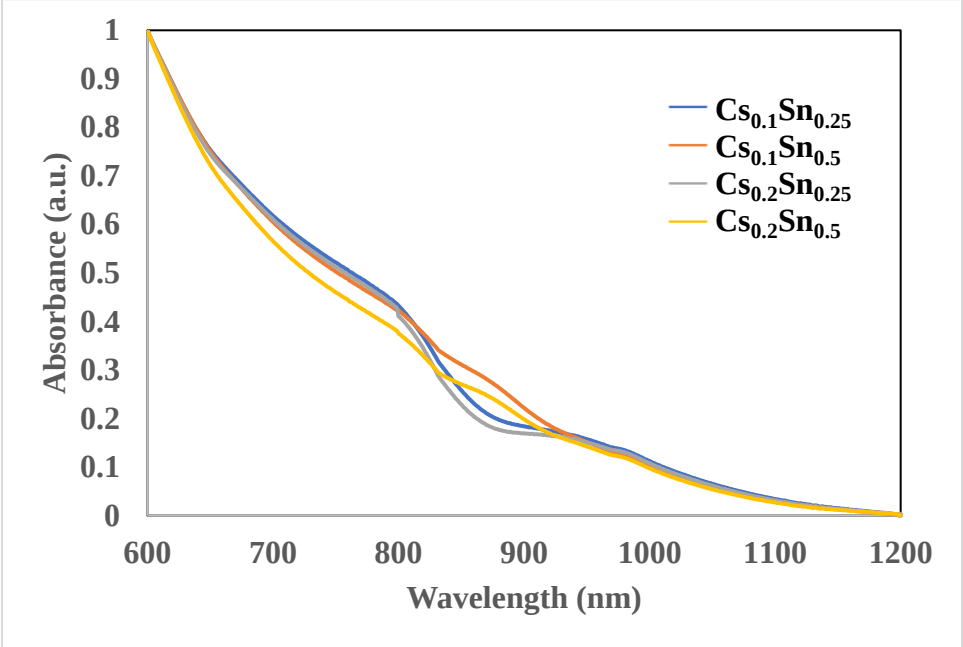

Figure 3. 4. UV-Vis spectra of $Cs_x(MA_{0.83}FA_{0.17})_{1-x}Pb_{1-y}Sn_y(I_{0.83}Br_{0.17})_3$ perovskite thin films with x = 0.1 and 0.2 and y = 0.25 and 0.5 with 700 µL toluene anti-solvent and a total concentration of 1 M.

These perovskite thin films were left in a petri dish in ambient air to test film air stability. XRD patterns of the films were taken after 10 days in air and compared to those of freshly made films (Figure 3.5). There were no extra oxidation peaks as reported due to the oxidation from Sn^{2+} to Sn^{4+}. In some previous reported literatures, the addition of Cs suppressed the Sn oxidation and stabilized the thin films. The perovskites exposed to air all have a slight left shift, which indicated a decrease in 2θ and an increase in d-spacing. This could attribute to a phase segregation in the perovskite layer.

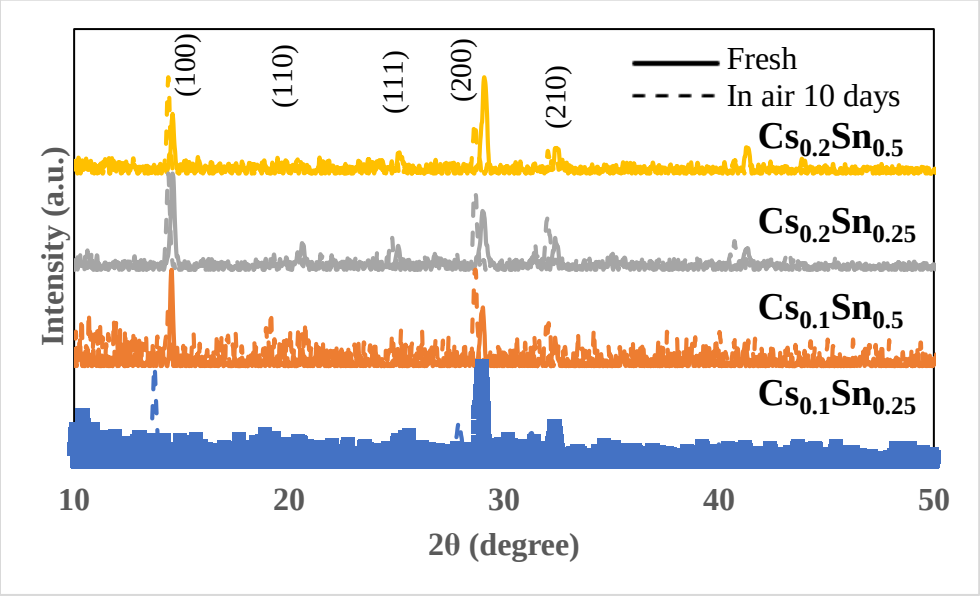

Figure 3. 5. X-Ray Diffraction patterns of $Cs_x(MA_{0.17}FA_{0.83})_{1-x}Pb_{1-y}Sn_y(I_{0.83}Br_{0.17})_3$ perovskite thin films with x = 0.1 and 0.2 and y = 0.25 and 0.5 fabricated with 700 µL toluene anti-solvent and a total concentration of 1 M. Fresh films are in solid lines and 10 days air exposure samples are in dotted lines.

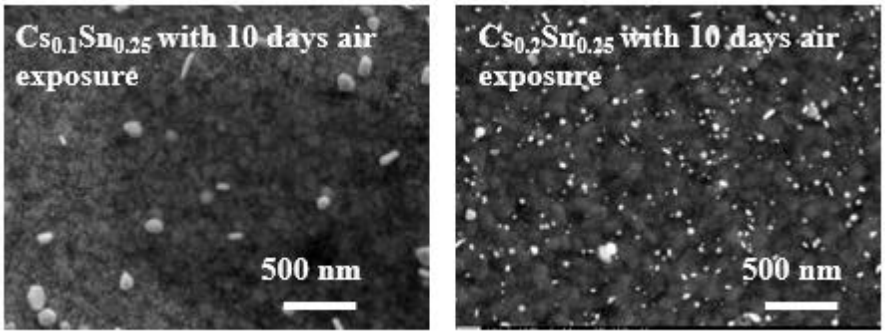

Figure 3. 6. SEM images of $Cs_x(MA_{0.17}FA_{0.83})_{1-x}Pb_{0.75}Sn_{0.25}(I_{0.83}Br_{0.17})_3$ perovskite thin films with x = 0.1 and 0.2 fabricated with 700 µL toluene anti-solvent and a total concentration of 1 M after 10 days air exposure.

SEM images (Figure 3.6) show many white rods appearing at the grain boundaries indicating phase segregation as also shown in Figure 3.5 of the left shift of XRD patterns. We further conducted EDS analysis on the $Cs_{0.2}(MA_{0.17}FA_{0.83})_{0.75}Pb_{0.75}Sn_{0.25}(I_{0.83}Br_{0.17})_3$ perovskite thin film. EDS data were taken from white rods and background grains. The results are shown in Figure 3.7 and Table 2.

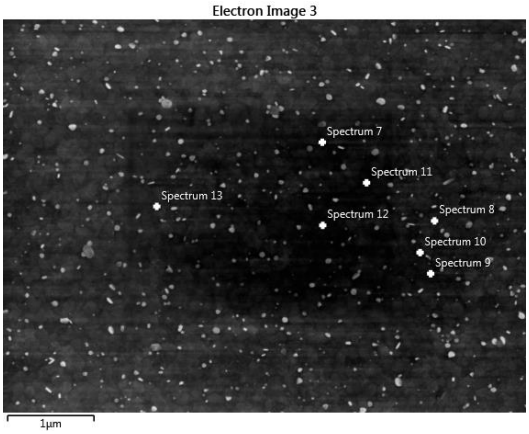

Figure 3. 7. SEM image of the $Cs_{0.2}(MA_{0.17}FA_{0.83})_{0.75}Pb_{0.75}Sn_{0.25}(I_{0.83}Br_{0.17})_3$ perovskite thin film, indicating the spots where EDS analysis conducted.

Table 2. The EDS measured average atomic percentage of elements on rods and background from the $Cs_{0.2}(MA_{0.17}FA_{0.83})_{0.75}Pb_{0.75}Sn_{0.25}(I_{0.83}Br_{0.17})_3$ thin film after 10 days of air exposure.

	Cs	Pb	Sn	I	Br	F
Rods (%)	4.20±0.78	28.14±9.14	5.82±1.92	44.33±12.47	16.13±4.80	1.38±1.13
Background (%)	5.34±0.62	35.73±10.85	4.66±1.11	44.69±16.84	9.35±4.30	0.23±0.41

In comparison of the elements percentage in white spots and grains, fluoride (F), Sn and Br were higher in white spots, indicating that the white spots could be the segregations of SnF_2 and SnBr. These segregations resulted in the increase d-spacing observed in Figure 3.5.

Since fabricating perovskite thin films with a total concentration of 1 M produced thin (~200-300 nm) light brown-yellow, semi-transparent films, leading to less light absorption and thus low efficiency, we increased the precursor total concentration to 2.5 M. We also decreased the volume of toluene dropped on the perovskite as the increase of Sn composition instead of keeping the toluene volume constant at 500 µL.

Table 3. Photographs of freshly made $Cs_x(MA_{0.17}FA_{0.83})_{1-x}Pb_{1-y}Sn_y(I_{0.83}Br_{0.17})_3$ perovskite thin films with a total concentration of 2.5 M and with toluene anti-solvent 700, 600, 500 and 400 µL for y = 0.25, 0.5, 0.75 and 1.0, respectively.

	$Sn_{0.25}$	$Sn_{0.5}$	$Sn_{0.75}$	Sn_1
$Cs_{0.05}$	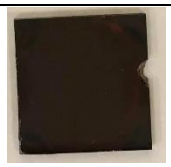	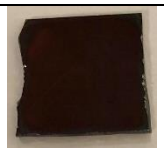		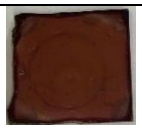
$Cs_{0.1}$	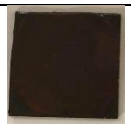		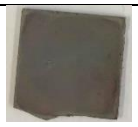	
$Cs_{0.2}$	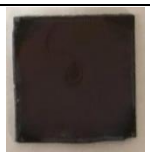	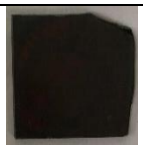	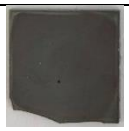	

With a total concentration of 2.5 M, the perovskite thin films have shiny uniform dark brown color as shown by their photographs in Table 3.

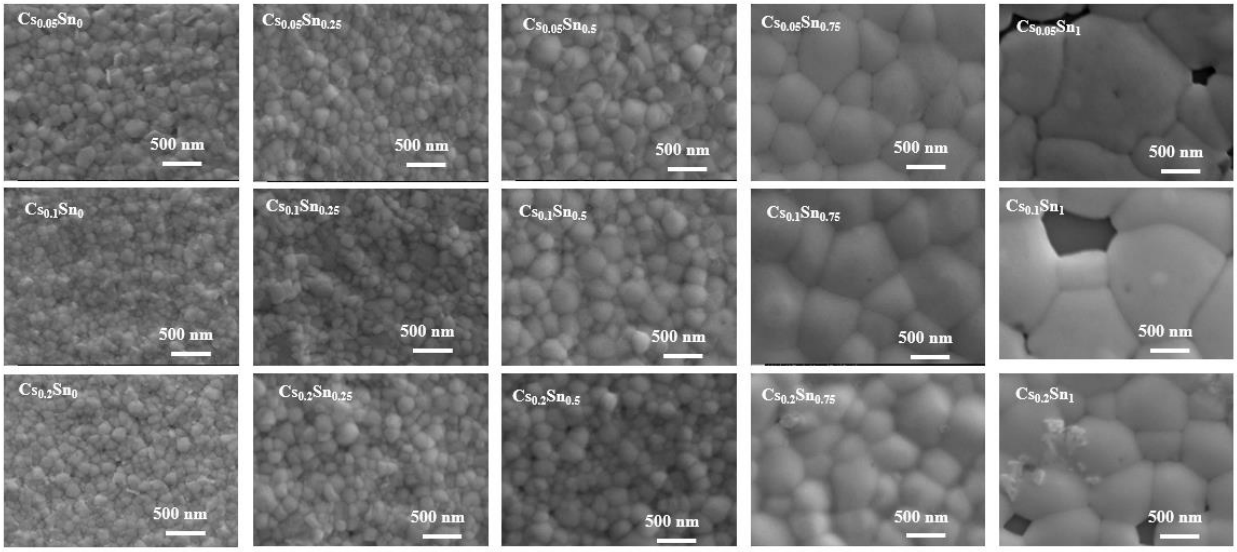

Figure 3. 8. SEM images of $Cs_x(MA_{0.17}FA_{0.83})_{1-x}Pb_{1-y}Sn_y(I_{0.83}Br_{0.17})_3$ perovskite thin films with x = 0.05, 0.1 and 0.2 and y = 0, 0.25, 0.5, 0.75, 1.0. The total concentration was 2.5 M. The volumes of toluene anti-solvent were 700 (y = 0,0.25), 600 (y = 0.5), 500 (y = 0.75) and 400 µL (y = 1.0).

Figure 3.8 shows all films are homogeneous and densely packed with clear grain boundaries. There was a slight increase in grain size when Sn composition increased from 0 % to 50 %, but a significant increase when Sn composition increased from 50 % to 75 %. This could possibly due to the slower crystallization which lead to the growth of grains. When Sn composition reached 100 %, the films were unable to obtain pinhole free due to the fast formation of grains, causing the grains unable to grow and spread uniformly across the whole film.

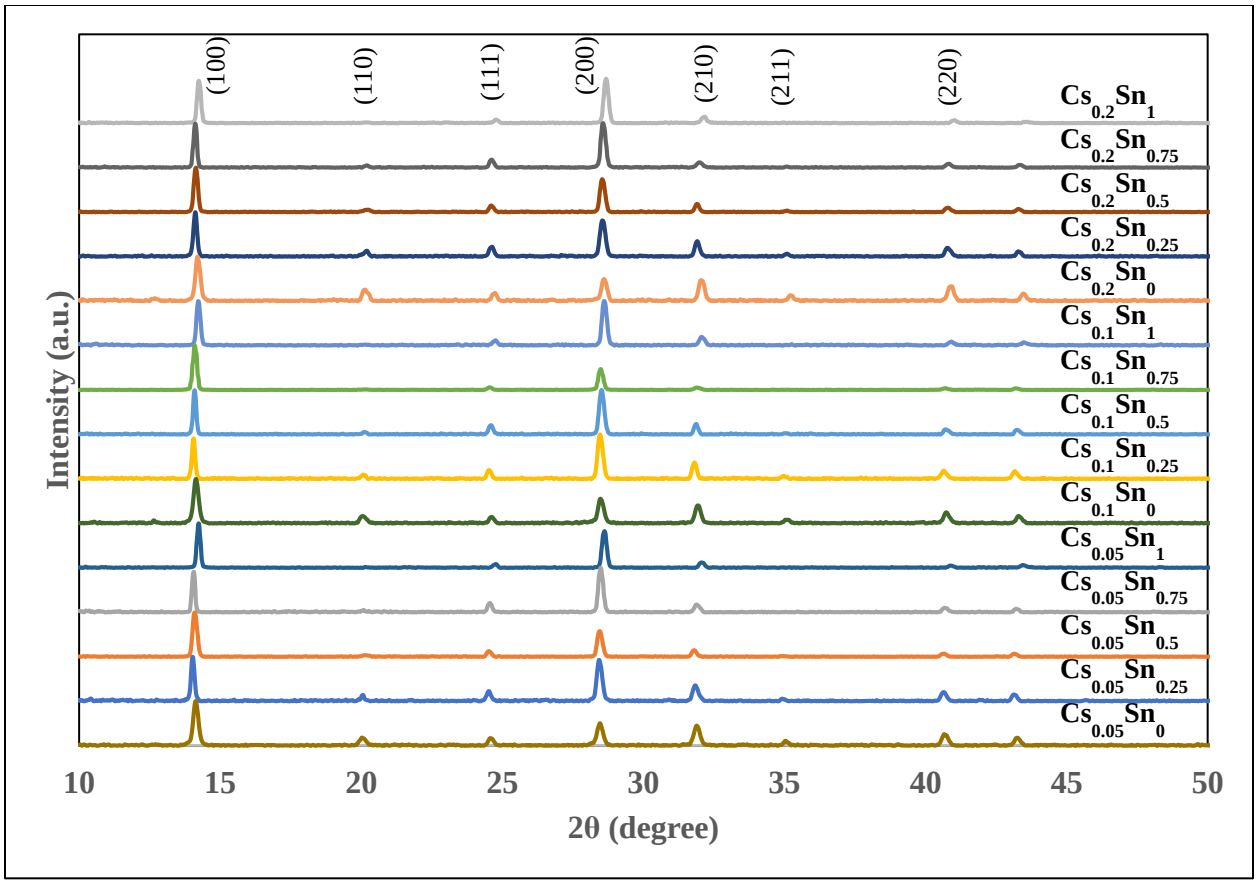

Figure 3. 9. XRD patterns of $Cs_x(MA_{0.17}FA_{0.83})_{1-x}Pb_{1-y}Sn_y(I_{0.83}Br_{0.17})_3$ perovskite thin films with x = 0.05, 0.1 and 0.2 and y = 0, 0.25, 0.5, 0.75, 1.0. The total concentration was 2.5 M. The volumes of toluene anti-solvent were 700 (y = 0,0.25), 600 (y = 0.5), 500 (y = 0.75) and 400 µL (y = 1.0).

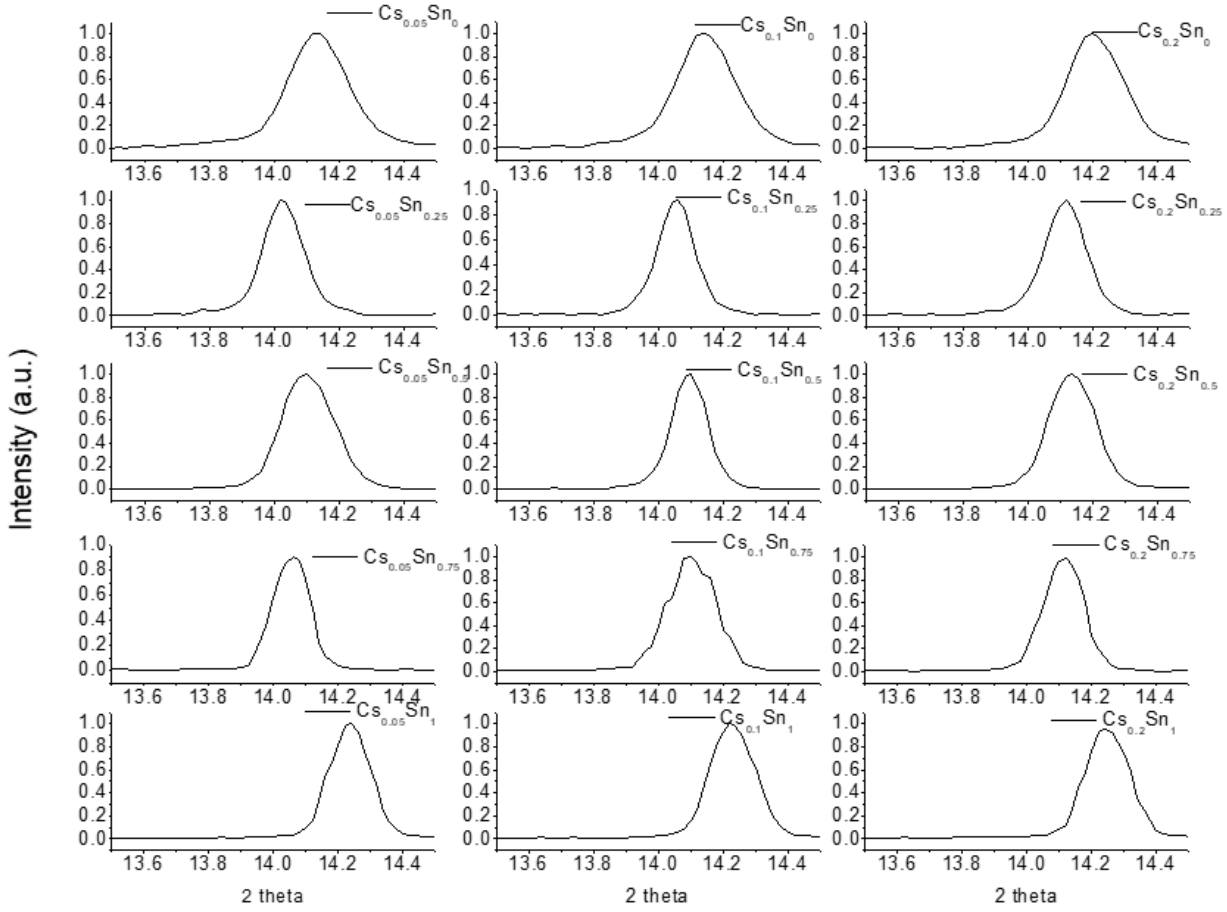

Figure 3. 10. The (100) plane peak from the XRD patterns of $Cs_x(MA_{0.17}FA_{0.83})_{1-x}Pb_{1-y}Sn_y(I_{0.83}Br_{0.17})_3$ perovskite thin films with x = 0.05, 0.1 and 0.2 and y = 0, 0.25, 0.5, 0.75, 1.0.

XRD patterns in Figure 3.9 show there are no contamination peaks as the Sn composition increases, but the (110) and (211) peaks disappeared when Sn composition was increased to 75%. To clearly show the shift in XRD patterns with the addition of Cs and Sn in the perovskite composition, the (100) plane peaks were displayed in Figure 3.10. There was a significant right shift when increasing the Cs composition from 5 % to 20 %, indicating a decrease in the d-spacing due to the smaller ion radius of Cs. The ion radii of the cations are MA^+ (2.7 Å), FA^+ (2.79 Å), and Cs^+ (1.67 Å) [15]. However, with the increase of Sn composition, there has no significant peak shift due to the similar radii of Pb^{2+} (1.19 Å) and Sn^{2+} (1.18 Å).

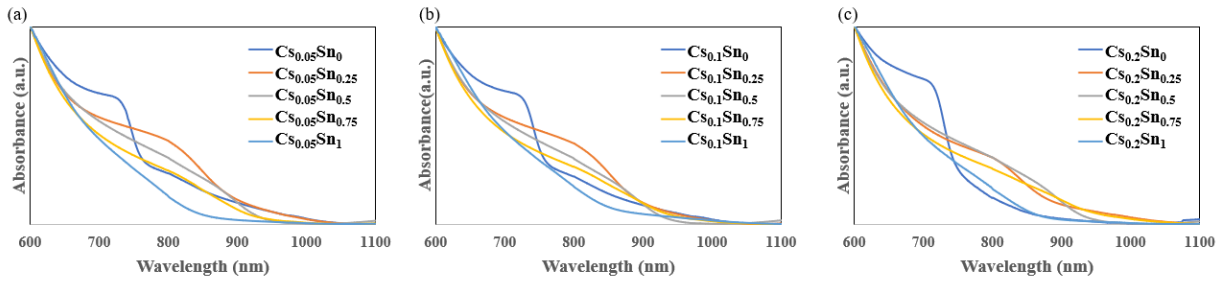

Figure 3. 11. UV- Vis spectra of $Cs_x(MA_{0.17}FA_{0.83})_{1-x}Pb_{1-y}Sn_y(I_{0.83}Br_{0.17})_3$ perovskite thin films with x = 0.05, 0.1 and 0.2 and y = 0, 0.25, 0.5, 0.75, 1.0. The total concentration was 2.5 M. The volumes of toluene anti-solvent were 700 (y = 0,0.25), 600 (y = 0.5), 500 (y = 0.75) and 400 µL (y = 1.0).

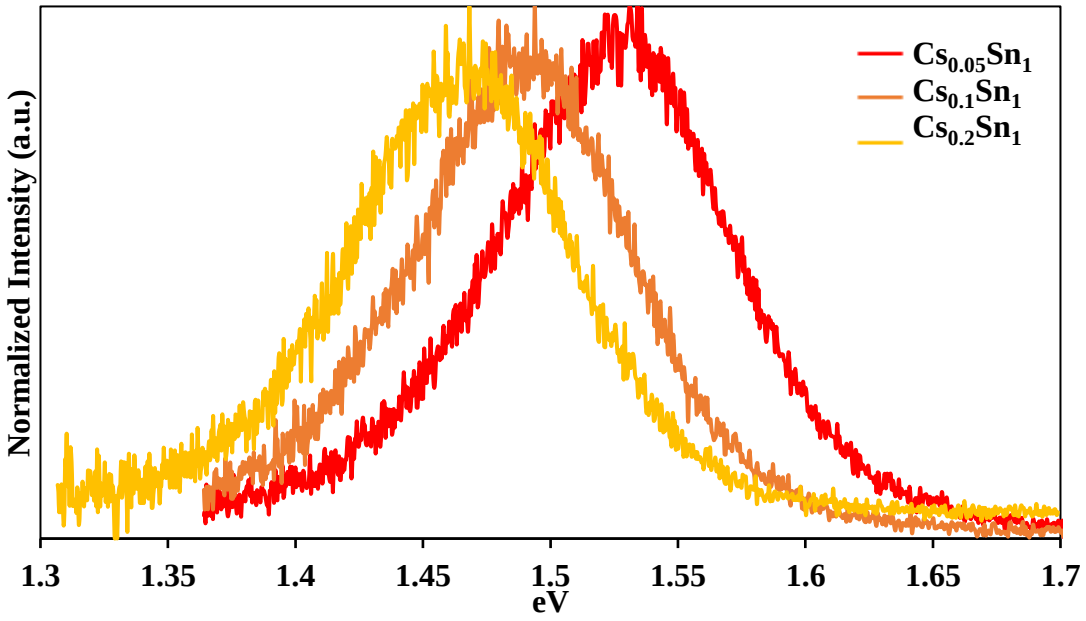

Figure 3. 12. Photoluminescence (PL) spectra of $Cs_x(MA_{0.17}FA_{0.83})_{1-x}Sn(I_{0.83}Br_{0.17})_3$ perovskite thin films with x = 0.05, 0.1 and 0.2 fabricated with a total concentration of 2.5 M and addition of SnF_2.

Due to the soften of band edge when increasing Sn composition in perovskites, the band edge became unable to determine from the UV-Vis spectra (Figure 3.11). To better estimate the bandgap of Cs_xSn_1 films, we collected their PL spectra with an excitation of 532 nm, shown in

Figure 3.12. In Figure 3.13, the bandgaps determined from the UV-Vis band edges and PL (pure Sn films) were plotted as a function of Sn composition for three Cs contents. For $Cs_{0.05}Sn_y$, the band gap decreases from a maximum of 1.60 eV ($Cs_{0.05}Sn_0$) to a minimum of 1.30 eV ($Cs_{0.05}Sn_{0.75}$) and then increases to 1.46 eV ($Cs_{0.05}Sn_1$). The similar trend is shown for 10 and 20 % Cs perovskites.

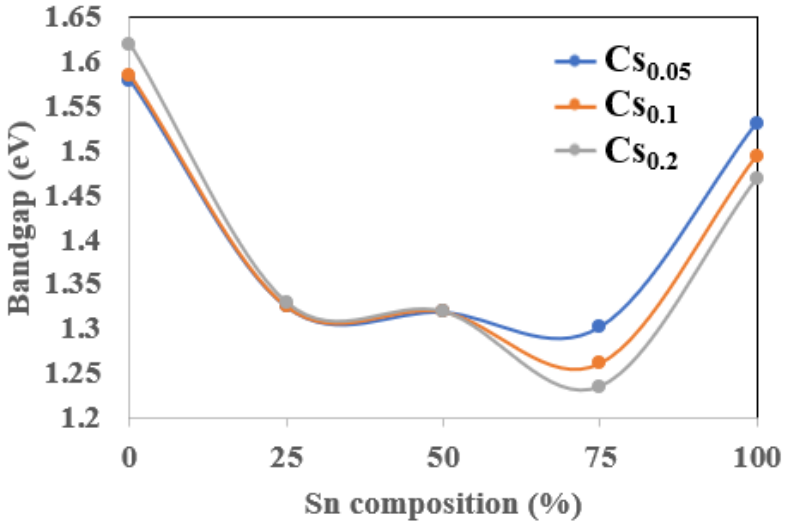

Figure 3. 13. Bandgap of perovskite thin films as a function of Sn composition for 5, 10 and 20% Cs determined from UV-Vis absorption spectra and PL for pure Sn films.

3.1.2 Air Stability of $Cs_x(MA_{0.17}FA_{0.83})_{1-x}Pb_{1-y}Sn_y(I_{0.83}Br_{0.17})_3$ Perovskite Thin Films Fabricated with the Addition of SnF_2

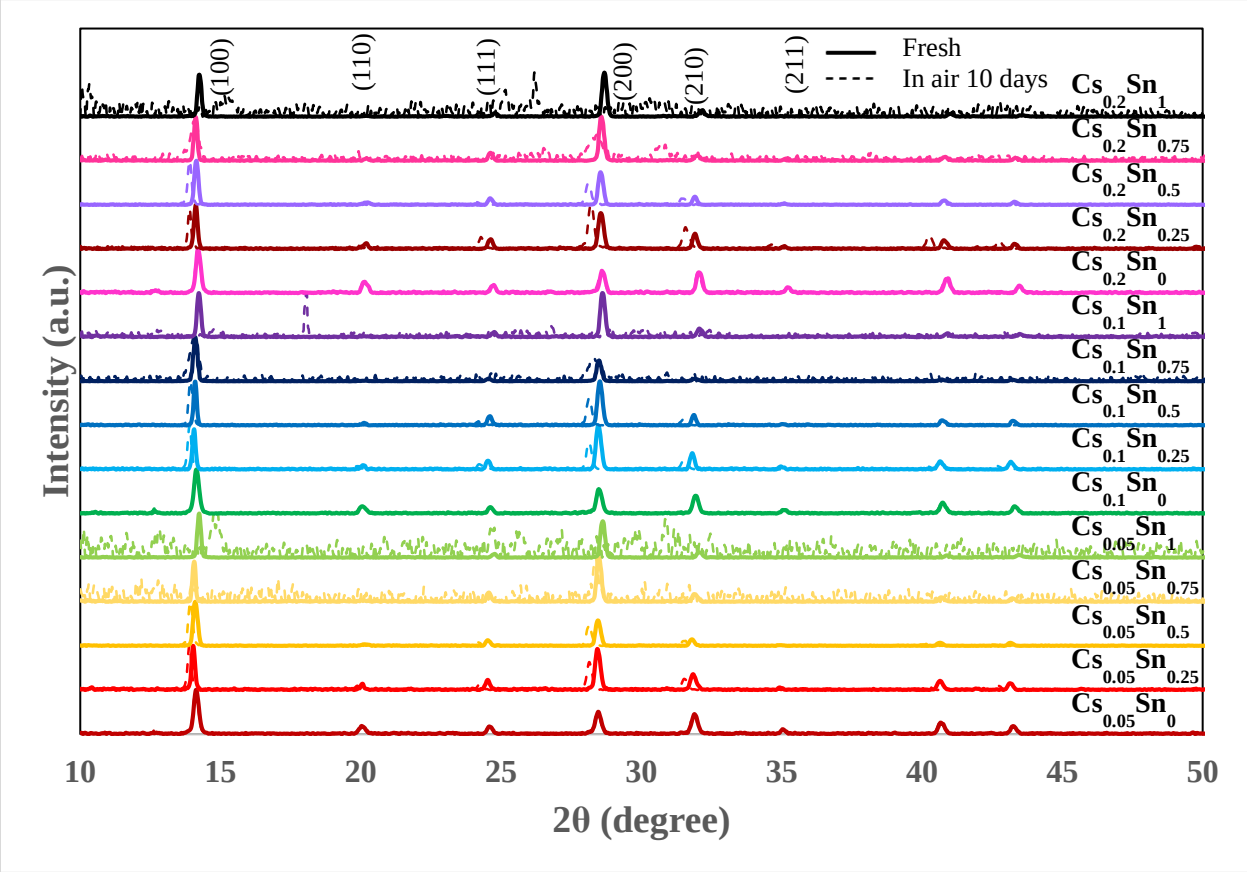

Figure 3. 14. XRD patterns of $Cs_x(MA_{0.17}FA_{0.83})_{1-x}Pb_{1-y}Sn_y(I_{0.83}Br_{0.17})_3$ perovskite thin films with x = 0.05, 0.1 and 0.2 and y = 0, 0.25, 0.5, 0.75, 1.0. The total concentration was 2.5 M. The volumes of toluene anti-solvent were 700 (y = 0,0.25), 600 (y = 0.5), 500 (y = 0.75) and 400 µL (y = 1.0). Fresh films are in solid line and 10 days air exposure are in dotted lines.

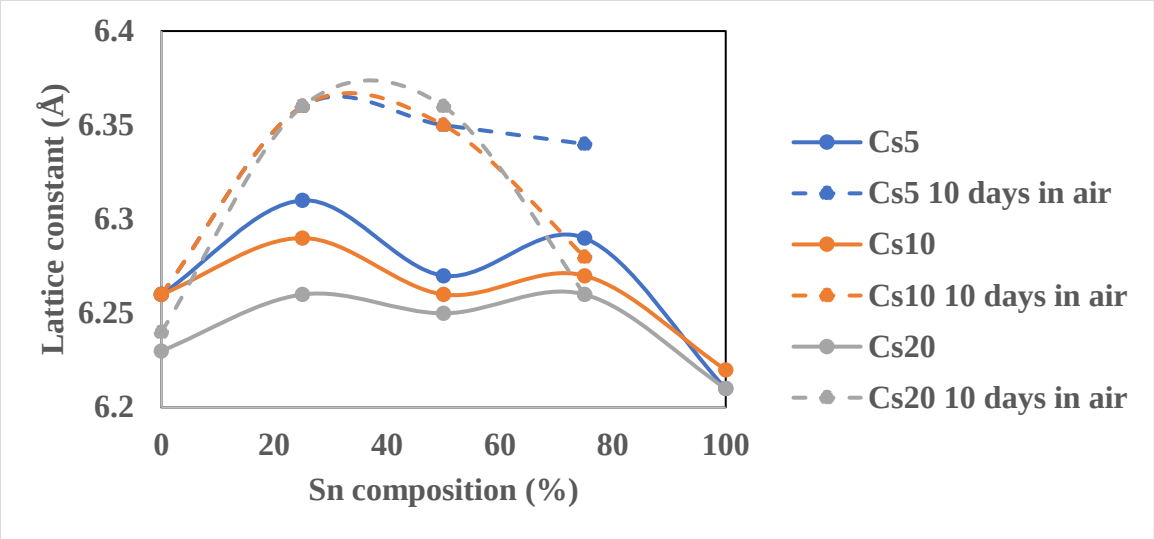

Figure 3. 15. Lattice parameters of fresh and 10 days air exposure perovskite thin films as a function of Sn composition for 5, 10 and 20% Cs determined from X-ray diffraction patterns.

As the increase in Sn composition, the left shift of XRD patterns became more obvious in Figure 3.14 after 10 days air exposure, indicating a more significant increase in d- spacing. The increasing of left shift could possibly be due to the segregation of SnF_2 from the film, since the amount of SnF_2 was increased accordingly to 10% per molar weight of SnI_2. In Figure 3.15, the lattice parameters of the films that were freshly made and after 10 days air exposure were calculated by Bragg's Law and plotted as a function of Sn for three Cs contents. Due to the increase composition of Sn, there were different degrees of phase segregation happening in the perovskite thin films, which caused the increase of lattice parameters. The phase segregation was suspected to be the segregates of SnF_2 and $SnBr_2$ since the peaks shifted to lower theta degree, the composition left in the perovskites were those with larger ion radii. From the XRD patterns in Figure 3.14, the lattice parameters of pure Sn films were not able to calculate due to the peak shifts or elimination of the (100) peak. The SEM images of the films after 10 days air exposure (Figure 3.16) show white rods on all films due to phase segregation, which confirms the peak shifts in the XRD patterns after 10 days air exposure.

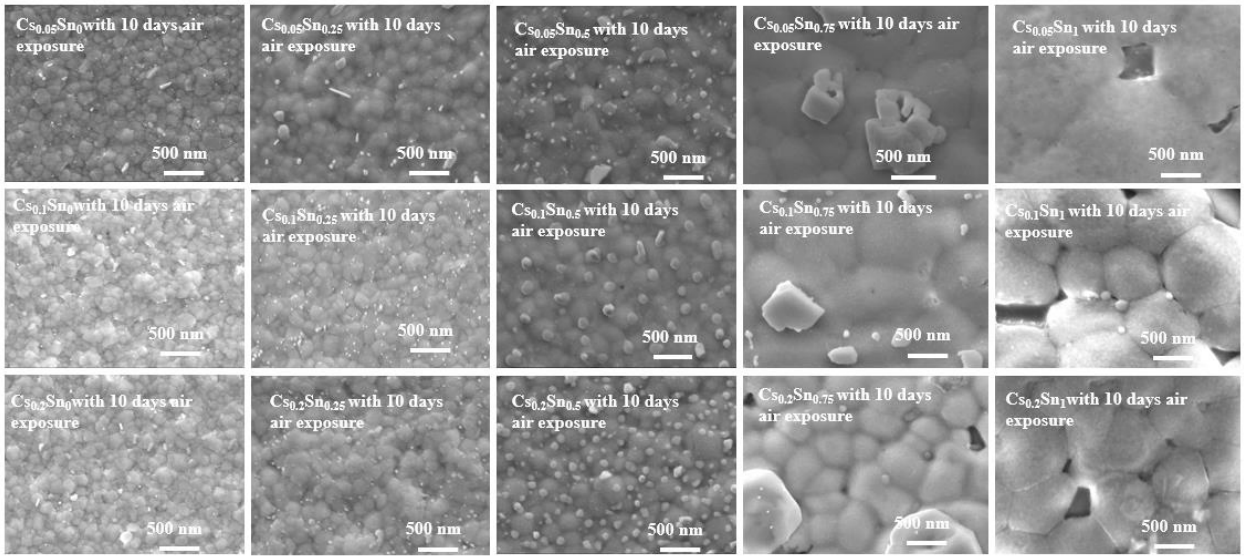

Figure 3. 16. SEM images of $Cs_x(MA_{0.17}FA_{0.83})_{1-x}Pb_{1-y}Sn_y(I_{0.83}Br_{0.17})_3$ perovskite thin films with x = 0.05, 0.1 and 0.2 and y = 0, 0.25, 0.5, 0.75, 1.0. The total concentration was 2.5 M. The volumes of toluene anti-solvent were 700 (y = 0,0.25), 600 (y = 0.5), 500 (y = 0.75) and 400 µL (y = 1.0).

3.1.3 $Cs_x(MA_{0.17}FA_{0.83})_{1-x}Pb_{1-y}Sn_y(I_{0.83}Br_{0.17})_3$ Perovskite Thin Films Fabricated with the Addition of SnF_2 and Variation in Anti- Solvent Volumes and Annealing Conditions

We observed that if we dropped the toluene anti-solvent in a flash, it would cause the toluene to wash away not only the excess DMSO, but also the perovskite, leaving a transparent circle in the middle of the film. To improve the film quality, we performed three diverse trials of dropping the toluene during the second spin coating. The first trial was dropping toluene during the last 15 s in a flash, the second trial was dropping toluene during the last 15 s but slowly and constantly over the span of 15 s, and the last trial was dropping toluene during the last 20 s slowly and constantly over the span of 20 s. The SEM images were taken to examine the surface morphology of the perovskite thin films in the trials and the SEM images are shown in Figure 3.17. The third trial of dropping toluene during the last 20 s and constantly dripping it for one

full second seems to have a poorer surface morphology than dropping toluene during the last 15 s. However, whether dropping toluene during the last 15 s in a flash or constantly dripping for one full second, the SEM images do not show a significant difference.

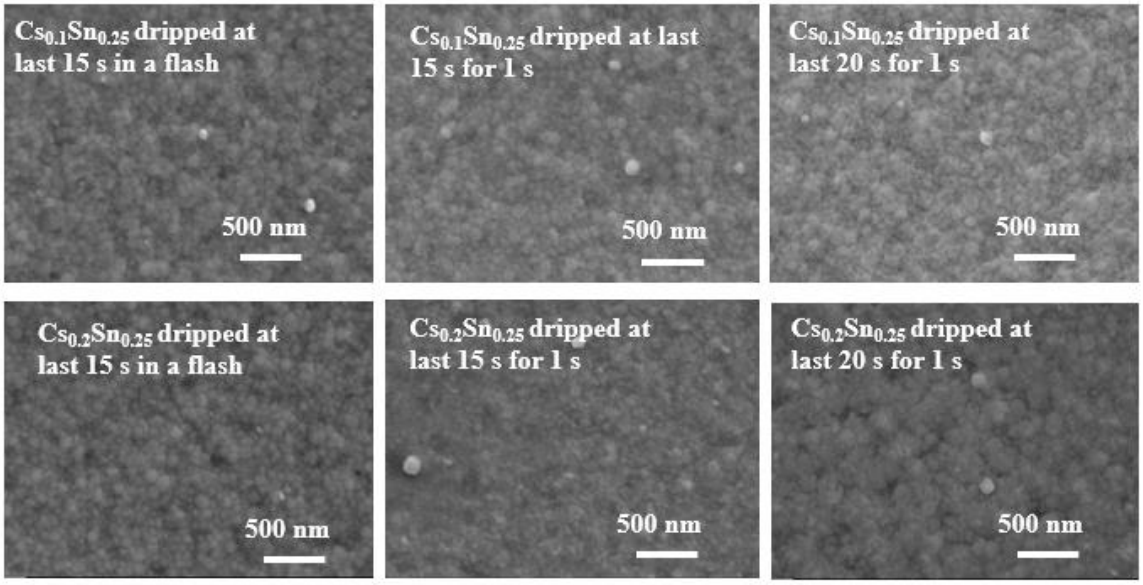

Figure 3. 17. SEM images of $Cs_x(MA_{0.17}FA_{0.83})_{1-x}Pb_{0.75}Sn_{0.25}(I_{0.83}Br_{0.17})_3$ perovskite thin films with a total concentration of 2.5 M with x = 0.1 and 0.2 with different dripping methods using 700 µL toluene anti-solvent.

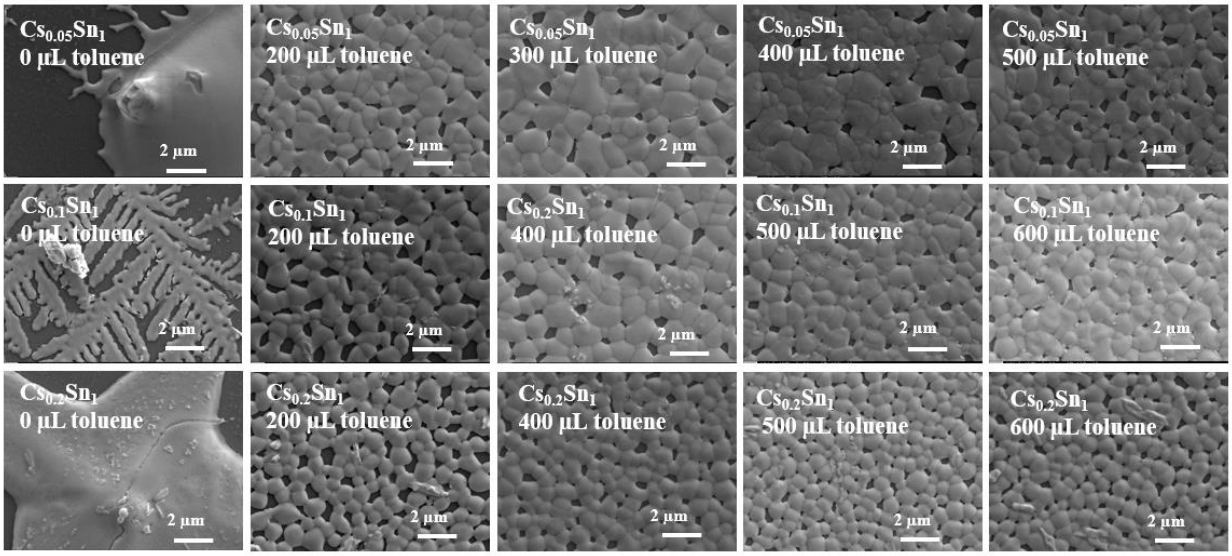

Figure 3. 18. SEM images of $Cs_x(MA_{0.17}FA_{0.83})_{1-x}Sn(I_{0.83}Br_{0.17})_3$ perovskite thin films with a total concentration of 2.5 M and different volumes of toluene anti-solvent.

To obtain uniform and pinhole-free 100 % Sn perovskite films, we changed the volume of toluene anti-solvent. SEM images (Figure 3.18) show no grains were formed if no toluene anti-solvent wash step was applied. Some grains were formed with 200 µL toluene, but with prominent pinholes all over the surface. As the volume of toluene anti-solvent was increased, the pinholes were decreased, but they were still visible on the films. Dropping 500 µL toluene on the perovskite film could result in the least pinholes on the 100 % Sn composition perovskite films for future film characterization, device fabrication and performance tests.

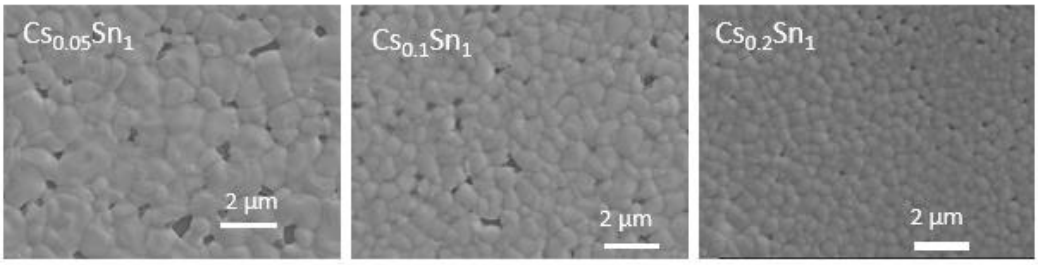

Figure 3. 19. SEM images of $Cs_x(MA_{0.17}FA_{0.83})_{1-x}Sn(I_{0.83}Br_{0.17})_3$ perovskite thin films with a total concentration of 2.5 M with x = 0.05, 0.1 and 0.2 with 500 µL toluene anti-solvent.

After modifying the toluene volume and changing the source of Br from $SnBr_2$ to FABr, pure Sn perovskite films had significantly less pinholes and clear grain boundaries. The change of Br source was due to the lower purity of $SnBr_2$ (99.2 %). Also, the grains were more uniform shown in Figure 3.19 compared to Figure 3.8. To make further improvements on the 100 % Sn composition perovskite films, we tried to modify the annealing conditions by either increasing the annealing temperature or increasing the annealing time of the perovskites. The results of modified annealing conditions are shown in SEM images in Figure 3.20.

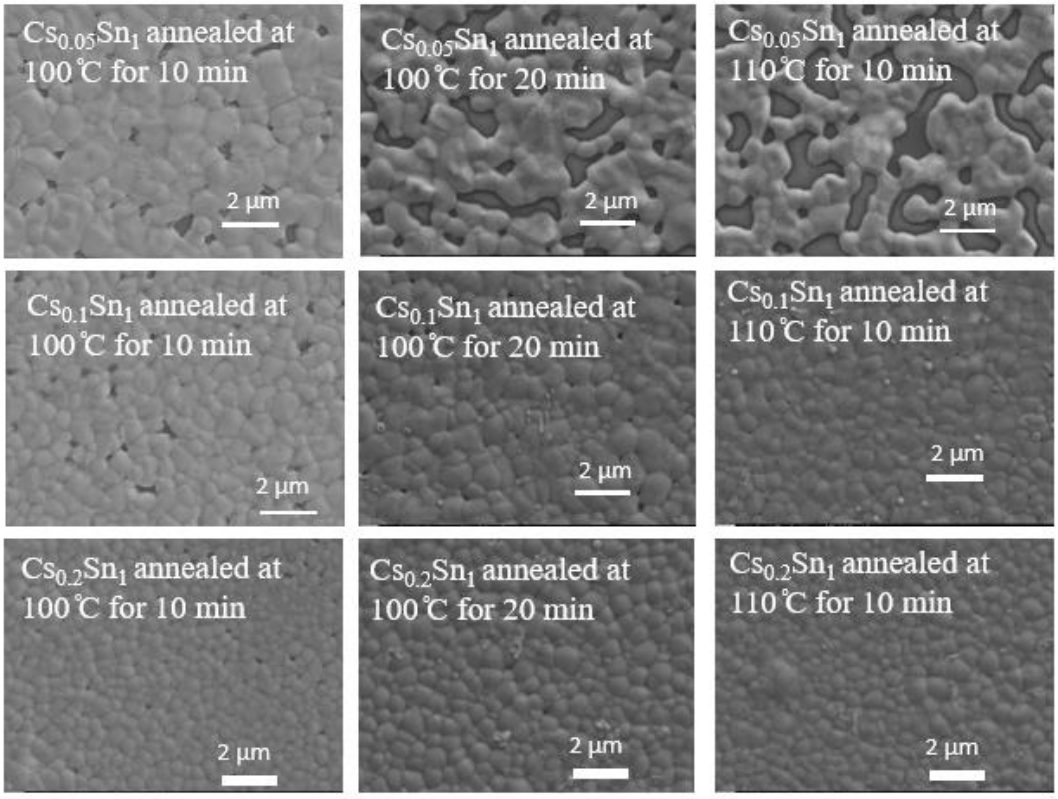

Figure 3. 20. SEM images of $Cs_x(MA_{0.17}FA_{0.83})_{1-x}Sn(I_{0.83}Br_{0.17})_3$ perovskite thin films with, x = 0.05, 0.1 and 0.2 fabricated with a total concentration of 2.5 M, 500 µL toluene anti-solvent and annealing at100℃ for 10 min, 100℃ for 20 min and 110℃ for 10 min.

We conducted two different trials, the first trial was keeping the annealing temperature constant at 100℃ but increasing the annealing time to 20 minutes and the second trial was

keeping the annealing time constant at 10 minutes but increasing the annealing temperature to 110℃. From the SEM images in Figure 3.20, the $Cs_{0.05}Sn_1$ films had a poorer grain formation than the original annealing conditions at 100℃ for 10 min, which could possibly result from the fast formation of grains at higher temperature, causing the grains unable to spread across the film before forming grains, leaving large pinholes. However, for the $Cs_{0.1}Sn_1$ and $Cs_{0.2}Sn_1$ films, the film morphologies were improved by varying the annealing conditions. We concluded that pinhole-free $Cs_{0.1}Sn_1$ and $Cs_{0.2}Sn_1$ films can be obtained by annealing at 110℃ for 10 min while at 100℃ for 10 min for $Cs_{0.05}Sn_1$. These conditions were used for future film characterizations and device fabrications. With the modified annealing conditions and toluene volume, we also took the SEM images of pure Sn films after 10 days air exposure to evaluate the air stability. As shown in Figure 3.21, after 10 days air exposure, large, light contrast grains appeared on the surfaces of Sn_1 perovskite thin films, indicting phase segregation.

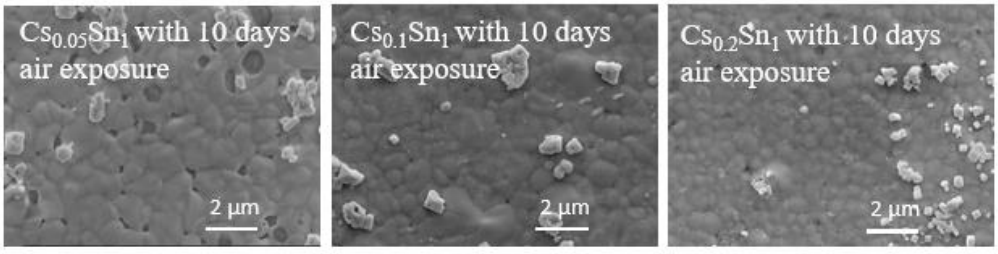

Figure 3. 21. SEM images of $Cs_x(MA_{0.17}FA_{0.83})_{1-x}Sn(I_{0.83}Br_{0.17})_3$ perovskite thin films with 10 days air exposure with x = 0.05, 0.1 and 0.2.

Since increasing annealing temperature from 100℃ to 110℃ resulted a denser $Cs_{0.2}Sn_1$ film, we attempted to reduce pinholes in $Cs_{0.2}Sn_{0.75}$ films by annealing at 110℃. However, the increase of annealing temperature resulted in an even worse morphology as shown in Figure 3.22 compared to that in Figure 3.8.

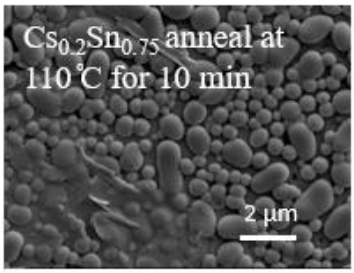

Figure 3. 22. SEM images of $Cs_{0.2}(MA_{0.17}FA_{0.83})_{0.8}Pb_{0.25}Sn_{0.75}(I_{0.83}Br_{0.17})_3$ perovskite thin films with anneal condition of 110℃ for 10 min.

3.1.4 $Cs_x(MA_{0.17}FA_{0.83})_{1-x}Pb_{1-y}Sn_y(I_{0.83}Br_{0.17})_3$ Perovskite Thin Films Fabricated Without the Addition of SnF_2

All precursors (MAI, FAI, PbI_2, $PbBr_2$ and SnI_2) were dissolved in a DMSO: GBL (3:7, v/v) co-solvent solution to a total concentration of 2.5 M. The reducing agent, SnF_2, was not added. The precursor solution was spin coated on a glass substrate at 500 rpm for 5 s, 1000 rpm for 15 s, and 4000 rpm for 40 s with a 700 μL toluene anti-solvent dropped during the last 15 s of the second spin coating step.

Table 4. The photographs of freshly made $Cs_x(MA_{0.17}FA_{0.83})_{1-x}Pb_{1-y}Sn_y(I_{0.83}Br_{0.17})_3$ perovskite thin films with x = 0, 0.05 and 0.1 and y = 0, 0.1 and 0.25, respectively, fabricated with a total precursor concentration of 2.5 M (no SnF_2) with 700 µL toluene anti-solvent

	Sn_0	$Sn_{0.1}$	$Sn_{0.25}$
Cs_0			
$Cs_{0.05}$		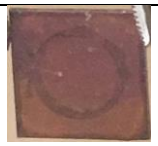	
$Cs_{0.1}$			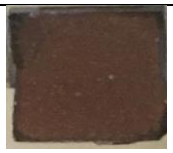

SEM images (Figure 3.23) show small grains, which are similar to the films fabricated with the addition SnF_2 (Figure 3.8). This might be due to the low Sn contents in the films. Without the addition of SnF_2, the lattice constant should increase, due to the increase of d-spacing since F^- has a smaller ionic radius of 1.33 Å, comparing to I^- (2.2 Å) and Br^- (1.96 Å) [15]. However, in Figure 3.25, the lattice constant decreased, this could due to the oxidation and degradation of the chemicals when measuring. Without the addition of SnF_2, there was an increase in bandgap (Figure 3.26) from the estimation of the UV- Vis absorption spectra (Figure 3.27).

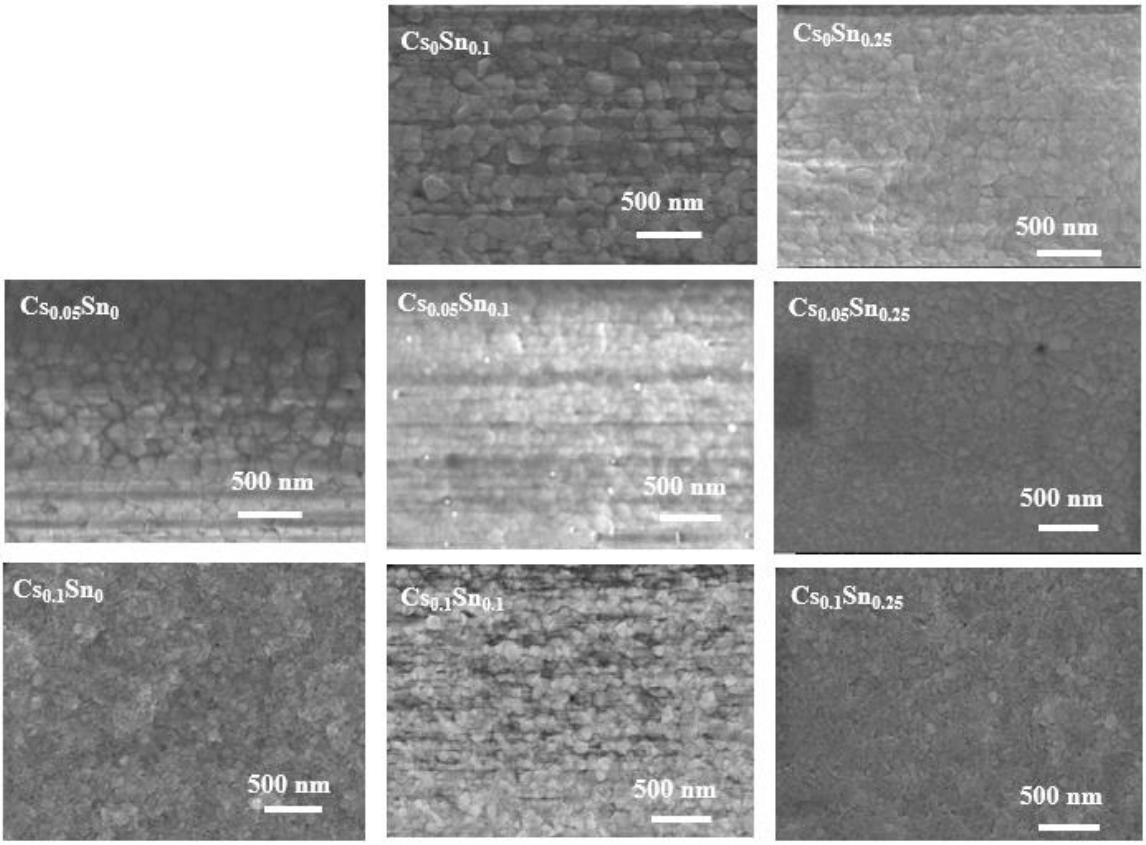

Figure 3. 23. SEM images of $Cs_x(MA_{0.17}FA_{0.83})_{1-x}Pb_{1-y}Sn_y(I_{0.83}Br_{0.17})_3$ perovskite thin films with x = 0, 0.05 and 0.1 and y = 0, 0.1 and 0.25, respectively, fabricated with a total precursor concentration of 2.5 M (no SnF_2) with 700 µL toluene anti-solvent. Images were taken with UHR mode.

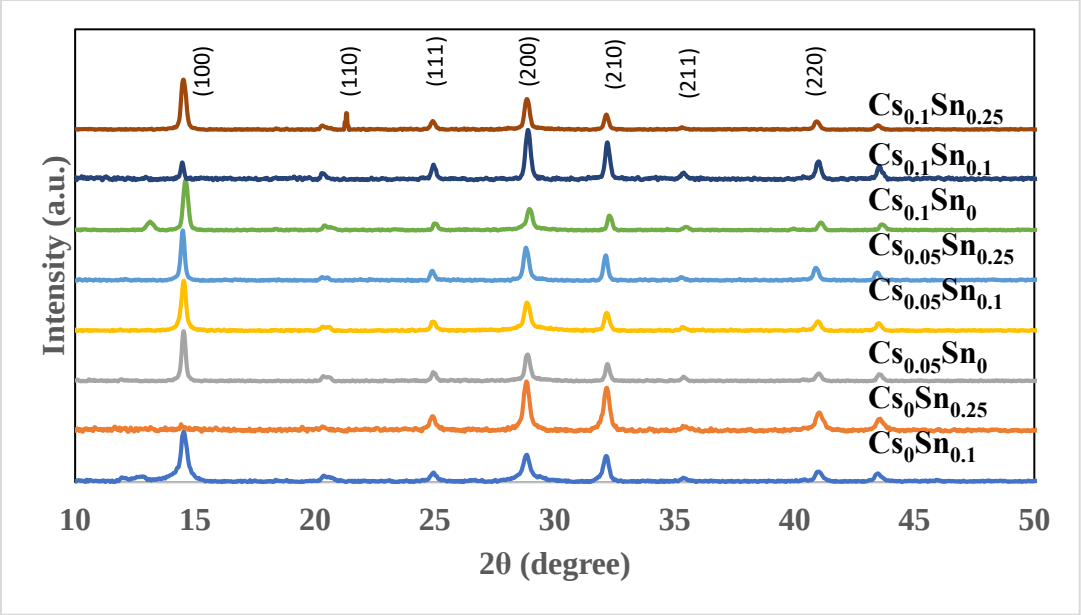

Figure 3. 24. XRD patterns of $Cs_x(MA_{0.17}FA_{0.83})_{1-x}Pb_{1-y}Sn_y(I_{0.83}Br_{0.17})_3$ perovskite thin films with x = 0, 0.05 and 0.1 and y = 0, 0.1 and 0.25, respectively, fabricated with a total precursor concentration of 2.5 M (no SnF_2), with 700 µL toluene anti-solvent.

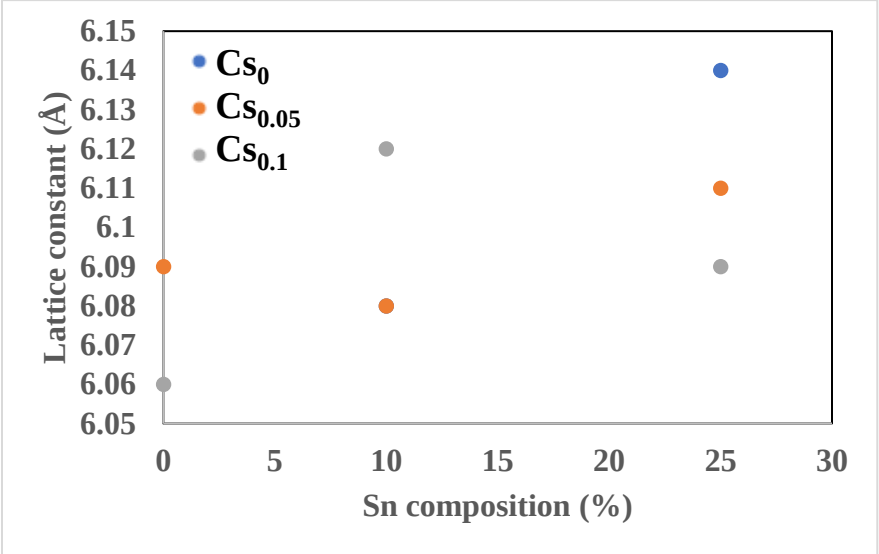

Figure 3. 25. Lattice constant of perovskite thin films as a function of Sn composition for 0, 5 and 10 % Cs determined from X-ray diffraction patterns.

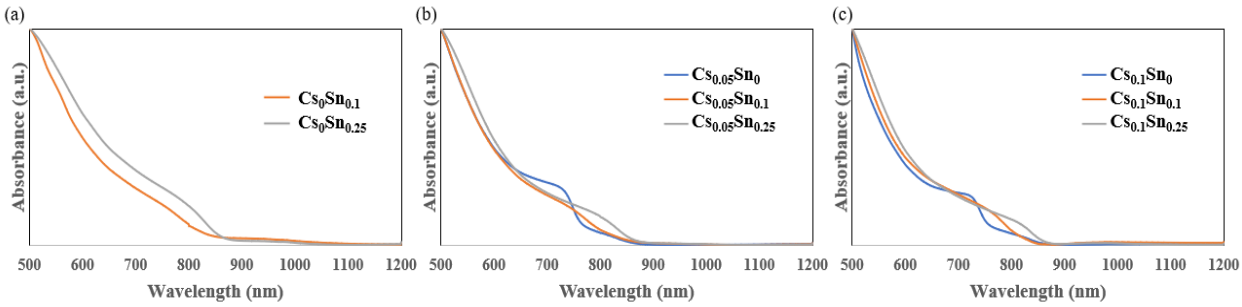

Figure 3. 26. UV-Vis spectra of $Cs_x(MA_{0.17}FA_{0.83})_{1-x}Pb_{1-y}Sn_y(I_{0.83}Br_{0.17})_3$ perovskite thin films with (a) x = 0, (b) x = 0.05 and (c) x = 0.1 and y = 0, 0.1 and 0.25, respectively, fabricated with a total precursor concentration of 2.5 M (no SnF_2), with 700 µL toluene anti-solvent.

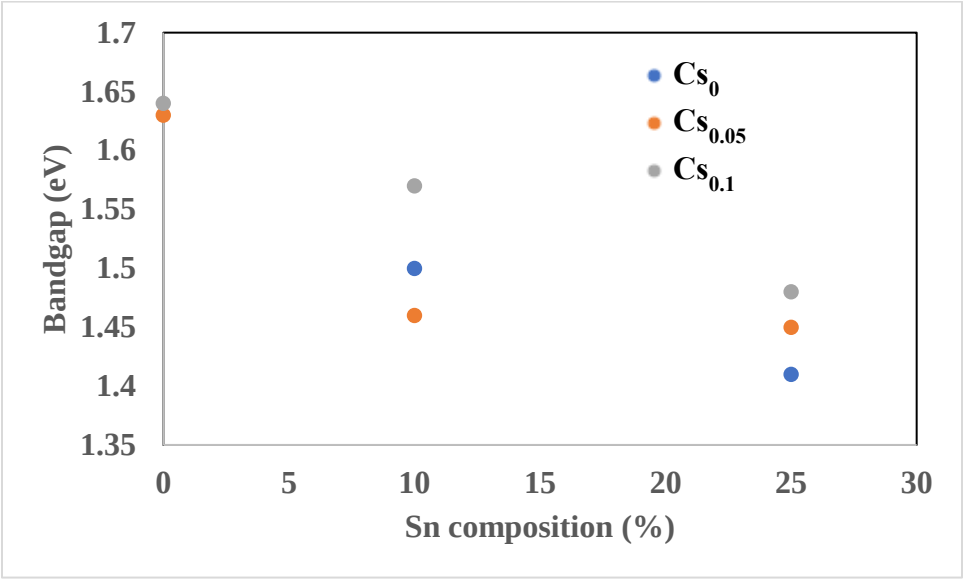

Figure 3. 27. Bandgap of perovskite thin films as a function of Sn composition for 0, 5 and 10 % Cs determined from UV-Vis absorption spectra.

We made a hypothesis that whether increasing the thermal annealing time would have impacts to morphology, structure and electronic properties of the perovskite thin films. We fabricated the $Cs_{0.05}(MA_{0.17}FA_{0.83})_{0.95}Pb_{0.9}Sn_{0.1}(I_{0.83}Br_{0.17})_3$ perovskite thin films with increasing thermal annealing time from 10 min to 60 min while keeping the thermal annealing temperature at 100℃.

With the increase of annealing time, no significant difference in film morphologies as shown in the SEM images (Figure 3.28). It could be that the grains were formed in the first 10 minutes of annealing, so without varying the annealing temperature, longer annealing has no influence on grains. From Figures 3.29 and 3.30, it is obvious that the XRD patterns and UV-Vis spectra have no difference with different annealing time. This proves that changing annealing time do not affect the crystallinity and the bandgap of the $Cs_{0.05}Sn_{0.1}$ perovskites.

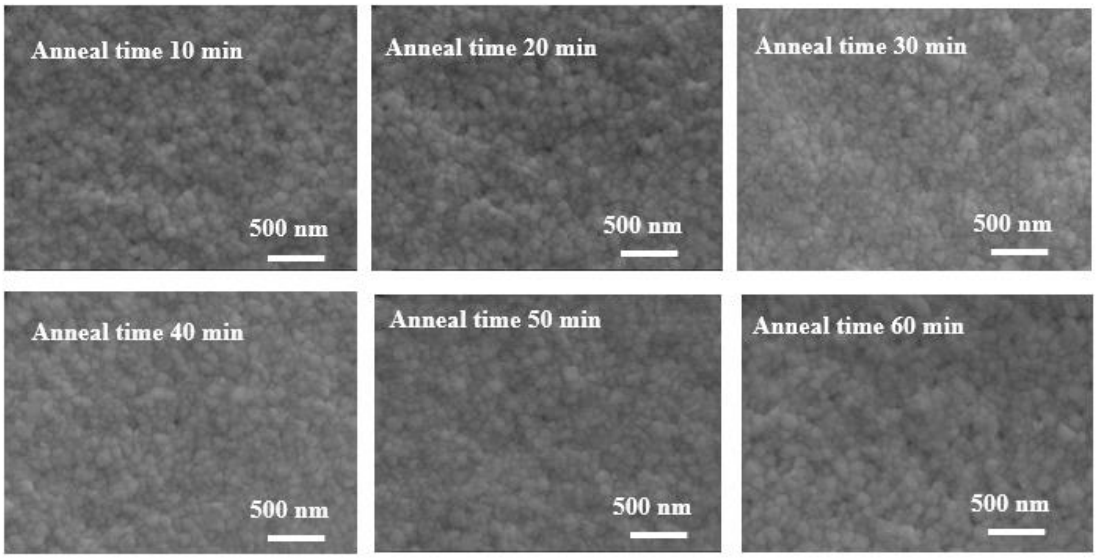

Figure 3. 28. SEM images of $Cs_{0.05}(MA_{0.17}FA_{0.83})_{0.95}Pb_{0.9}Sn_{0.1}(I_{0.83}Br_{0.17})_3$ perovskite thin films fabricated by annealing at 100℃ for different thermal annealing time. The toluene anti-solvent was 700 µL.

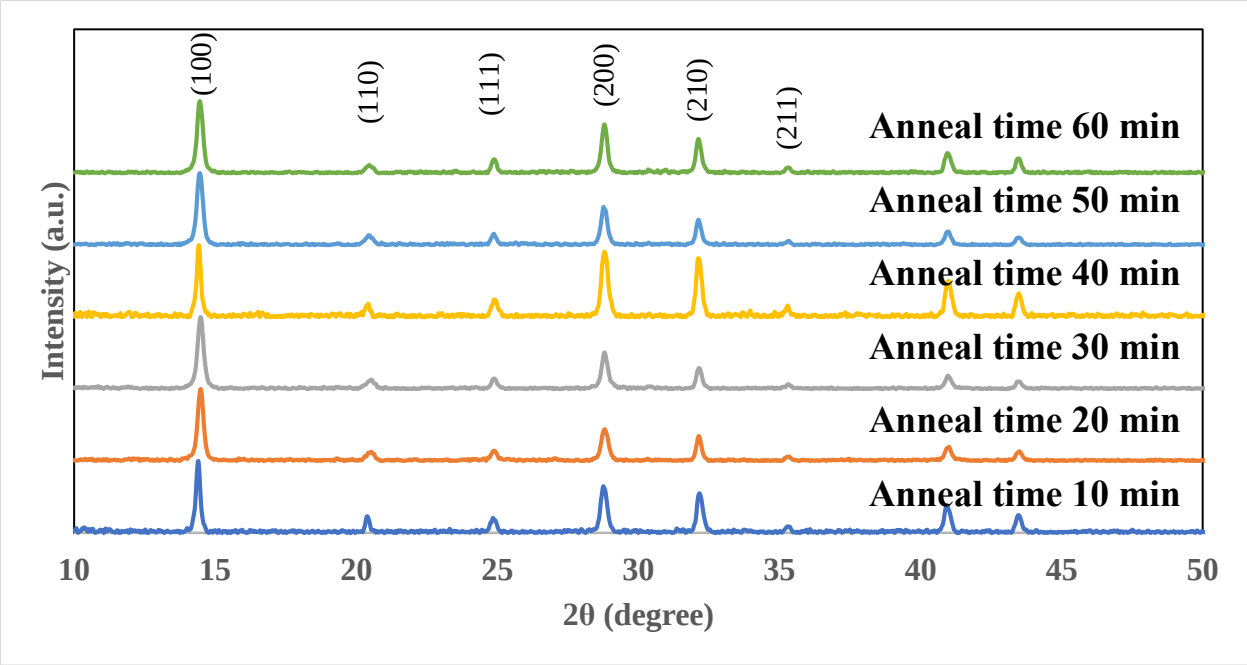

Figure 3. 29. X- Ray Diffraction (XRD) patterns of $Cs_{0.05}(MA_{0.17}FA_{0.83})_{0.95}Pb_{0.9}Sn_{0.1}(I_{0.83}Br_{0.17})_3$ perovskite thin films fabricated by annealing at 100℃ for different thermal annealing time Toluene anti-solvent was 700 µL.

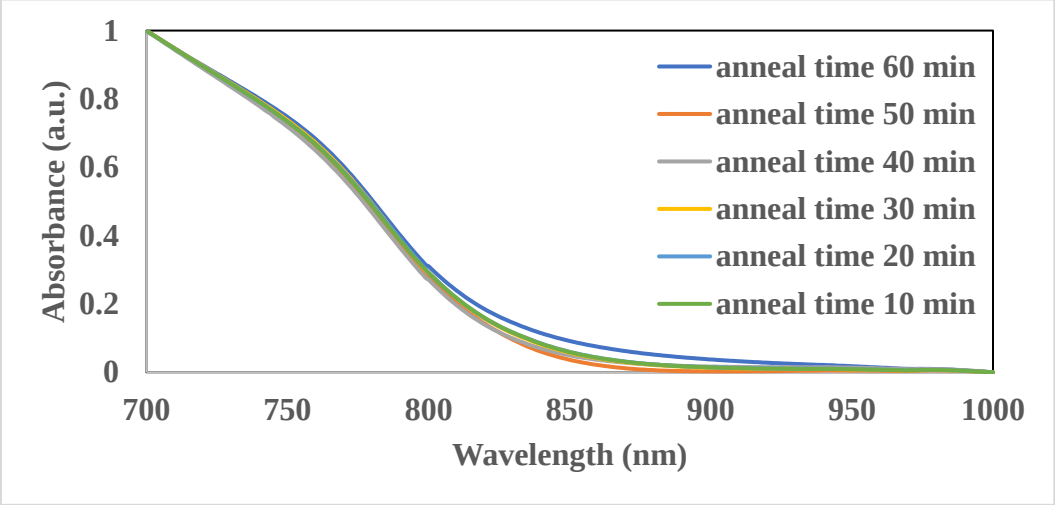

Figure 3. 30. UV-Vis spectra of $Cs_{0.05}(MA_{0.17}FA_{0.83})_{0.95}Pb_{0.9}Sn_{0.1}(I_{0.83}Br_{0.17})_3$ perovskite thin films fabricated by annealing at 100℃ for different thermal annealing time. Toluene anti-solvent was 700 µL.

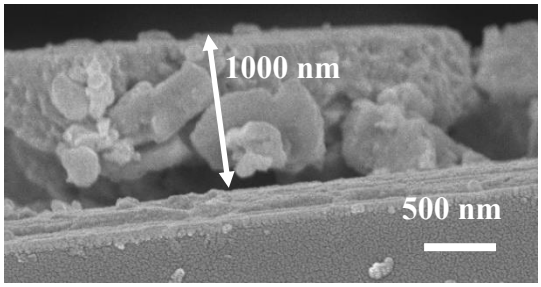

Figure 3. 31. Cross-section SEM images of $Cs_{0.05}(MA_{0.17}FA_{0.83})_{0.95}Pb_{0.9}Sn_{0.1}(I_{0.83}Br_{0.17})_3$ perovskite thin film fabricated by annealing at 100℃ for 10 min with 700 µL toluene anti-solvent.

The cross-section SEM image (Figure 3.31) shows that the film thickness is about 1000 nm for the $Cs_{0.05}(MA_{0.17}FA_{0.83})_{0.95}Pb_{0.9}Sn_{0.1}(I_{0.83}Br_{0.17})_3$ perovskite thin film annealed at 100C for xx min. Some holes are present between the perovskite layer and the glass substrate, which could be due to the unreachable of anti-solvent with the film made using a precursor solution of 2.5 M.

The tolerance factor for the $Cs_x(MA_{0.17}FA_{0.83})_{1-x}Pb_{1-y}Sn_y(I_{0.83}Br_{0.17})_3$ composition was 0.937. Perovskite solar cells with the perovskite films of a lower tolerance factor around 0.917 demonstrated good device performance [31]. While the devices we made with $Cs_x(MA_{0.17}FA_{0.83})_{1-x}Pb_{1-y}Sn_y(I_{0.83}Br_{0.17})_3$ films did not demonstrate satisfactory performance, we made hypothesis that reducing the tolerance factor might improve the performance. The radii of MA^+ (2.16 Å), FA^+ (2.53 Å), Cs^+ (1.67 Å), Pb^{2+} (1.19 Å), Sn^{2+} (1.15 Å), I^- (2.20 Å), and Br (1.96 Å) were used to calculate the tolerance factor. [11] To keep the tolerance factor of 0.917, the perovskites would have the compositions of $Cs_x(MA_{0.6}FA_{0.4})_{1-x}Pb_{0.9}Sn_{0.1}(I_{0.4}Br_{0.6})_3$ with x = 0 and 0.05. The following figures show the photographs, UV- Vis spectra, XRD patterns and SEM images of the perovskite films fabricated with different thermal annealing temperature and time, with 700 µL toluene anti-solvent and no SnF_2 was added in the precursor solutions.

Table 5. Photographs of fresh $Cs_x(MA_{0.6}FA_{0.4})_{1-x}Pb_{0.9}Sn_{0.1}(I_{0.4}Br_{0.6})_3$ perovskite thin films fabricated with different thermal annealing temperature and time, with 700 µL toluene anti-solvent and 2.5 M total precursor concentration without the addition of SnF_2.

	Thermal anneal at 100 ℃ for 60 min	Thermal anneal at 100 ℃ for 30 min	Thermal anneal at 100 ℃ for 10 min	Thermal anneal at 130 ℃ for 10 min
Cs_0	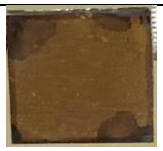		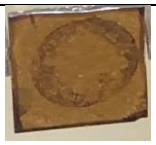	
$Cs_{0.05}$	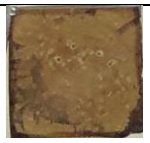	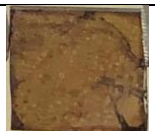		

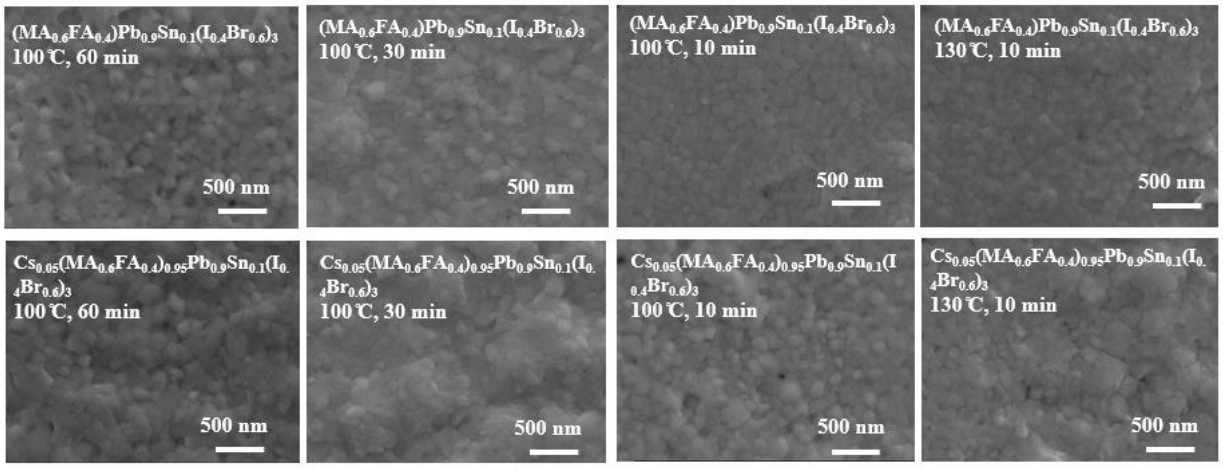

Figure 3. 32. SEM images of $Cs_x(MA_{0.6}FA_{0.4})_{1-x}Pb_{0.9}Sn_{0.1}(I_{0.4}Br_{0.6})_3$ perovskite thin films with x = 0 and 0.05 fabricated with different thermal annealing temperature and time, with 700 µL toluene anti-solvent and 2.5 M total precursor concentration without the addition of SnF_2.

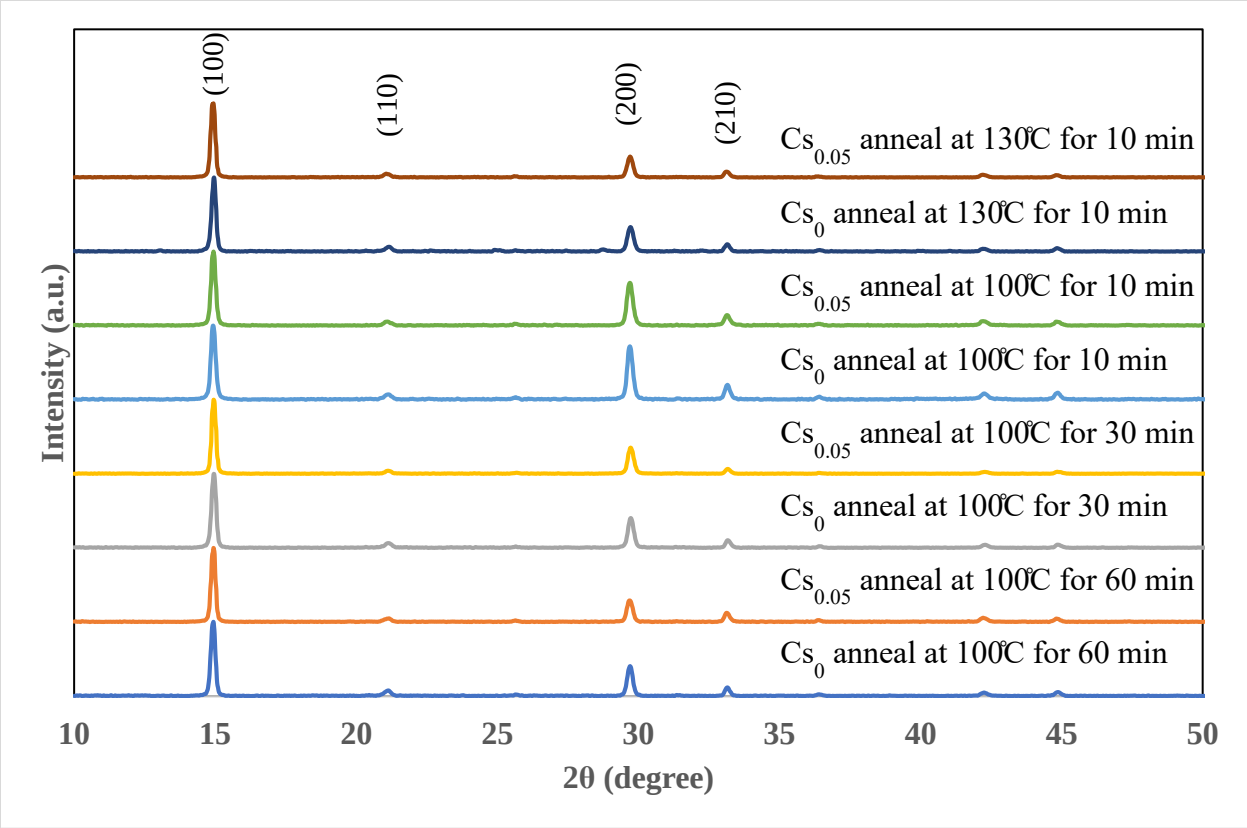

Figure 3. 33. XRD patterns of $Cs_x(MA_{0.6}FA_{0.4})_{1-x}Pb_{0.9}Sn_{0.1}(I_{0.4}Br_{0.6})_3$ perovskite thin films with x = 0 and 0.05 fabricated with different thermal annealing temperature and time, with 700 µL toluene anti-solvent and 2.5 M total precursor concentration without the addition of SnF_2.

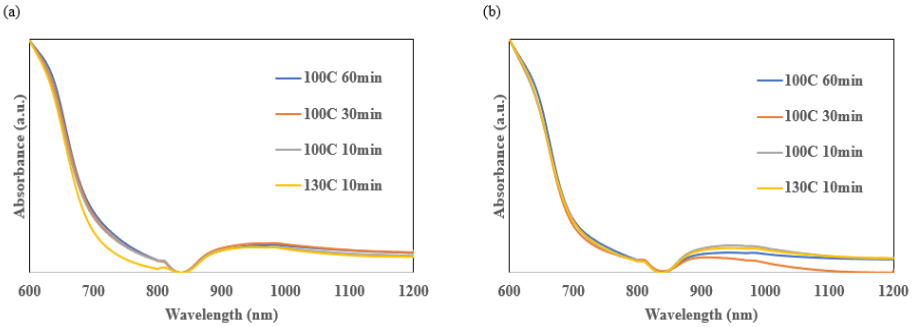

Figure 3. 34. UV-Vis spectra of $Cs_x(MA_{0.6}FA_{0.4})_{1-x}Pb_{0.9}Sn_{0.1}(I_{0.4}Br_{0.6})_3$ perovskite thin films with (a) x= 0 and (b) x = 0.05 fabricated with different thermal annealing temperature and time, with 700 µL toluene anti-solvent and 2.5 M total precursor concentration without the addition of SnF_2.

For the $Cs_x(MA_{0.6}FA_{0.4})_{1-x}Pb_{0.9}Sn_{0.1}(I_{0.4}Br_{0.6})_3$ films (x = 0, 0.05), SEM images (Figure 3.32) show the films annealed at 100 C for 10 min appear slightly better than other conditions in terms of grain uniformity and surface coverage. The XRD patterns (Figure 3.33) and the UV-Vis spectra (Figure 3.34) show no obvious difference with the addition of Cs or the increase of annealing time and temperature.

Apparently, the films with the composition of $Cs_x(MA_{0.6}FA_{0.4})_{1-x}Pb_{0.9}Sn_{0.1}(I_{0.4}Br_{0.6})_3$ (x = 0, 0.05) have light color (Table 5) than the films with the compositions of $Cs_x(MA_{0.17}FA_{0.83})_{1-x}Pb_{1-y}Sn_y(I_{0.83}Br_{0.17})_3$ (x = 0, 0.05 and 0.1 and y = 0, 0.1 and 0.25) (Table 4). They also have larger bandgaps (1.78-1.79 eV) and lattice constant (5.92 Å).

3.2 Perovskite Thin Films Fabricated with Mixed Solvent of DMF and DMSO with Chlorobenzene Anti- Solvent

To achieve uniform, dark color perovskite films, we use a one-step anti-solvent method. Reported in literature, co-solvent DMF: DMSO was used for making precursor solutions and chlorobenzene was used as an anti-solvent. [4] All precursors (MAI, FAI, PbI_2, $PbBr_2$, and SnI_2) were dissolved in a DMSO: DMF (1:4, v/v) co-solvent to a total concentration of 1 M and 2.5 M. The precursor solution was spin coated on a cleaned glass substrate at 1000 rpm for 10 s and 6000 rpm for 20 s with a 100 µL chlorobenzene anti-solvent dropped during the last 5 s of the second spin coating step.

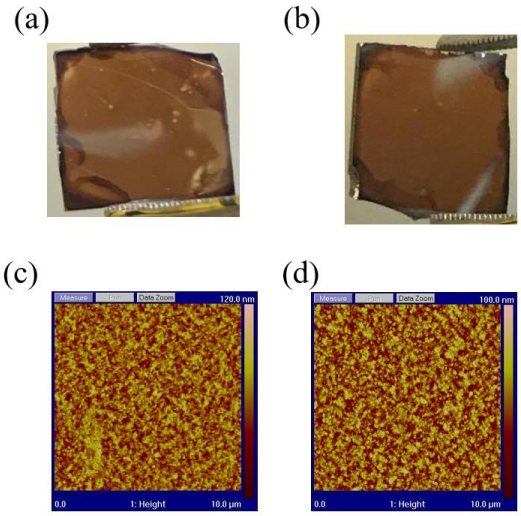

Figure 3. 35. The photographs (a, b) and AFM images (c. d) of $Cs_x(MA_{0.17}FA_{0.83})_{1-x}Pb(I_{0.83}Br_{0.17})_3$ perovskite thin films with a total concentration of 1 M with (a) x = 0 and (b) x = 0.05.

Photographs (Figures 3.35 (a) and (b)) show a more uniform film was obtained with the addition of 5 % Cs. The AFM topographic images (Figures 3.35 (c) and (d)) show that the addition of 5 % Cs decreased the roughness of the surface from 120 nm to 100 nm. Smoother surfaces could be a favor for the fabrication of perovskite solar cells since the subsequent layers are thermally evaporated on the perovskite films.

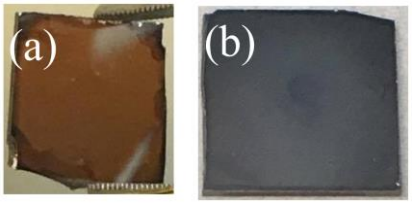

Figure 3. 36. The photographs of $Cs_{0.05}(MA_{0.17}FA_{0.83})_{0.95}Pb(I_{0.83}Br_{0.17})_3$ perovskite thin films with the total precursor concentration of (a) 1M and (b) 2.5 M.

When the total precursor concentration was increased from1 M to 2.5 M, a uniform, black color film was obtained, instead of a light brown transparent film (Figure 3.36).

Table 6. The photographs of fresh $Cs_x(MA_{0.17}FA_{0.83})_{1-x}Pb_{1-y}Sn_y(I_{0.83}Br_{0.17})_3$ perovskite thin films fabricated with 100 µL chlorobenzene anti-solvent and no SnF_2 in precursor solutions.

	Sn_0	**$Sn_{0.1}$**	**$Sn_{0.25}$**	**$Sn_{0.5}$**	**$Sn_{0.745}$**
Cs_0		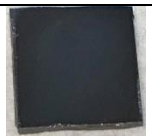			
$Cs_{0.05}$		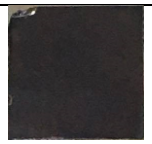			
$Cs_{0.1}$	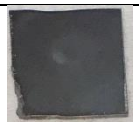		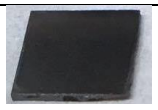	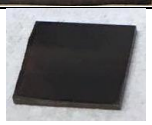	
$Cs_{0.2}$	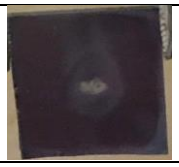				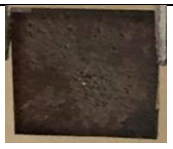

Due to the chemicals used for the precursors and the compositions of perovskites, to achieve $Br_{0.51}$ using $PbBr_2$, at least $Pb_{0.255}$ will be presented in the perovskites. Therefore, pure Sn perovskites cannot be achieved if using $PbBr_2$. We could only reach $Sn_{0.745}$. With the increase of Sn, the perovskite films became lighter color, and the more phase segregation from the uneven color contrast of the films shown in Table 6, which could be due to the quick oxidation of Sn^{2+} to Sn^{4+}.

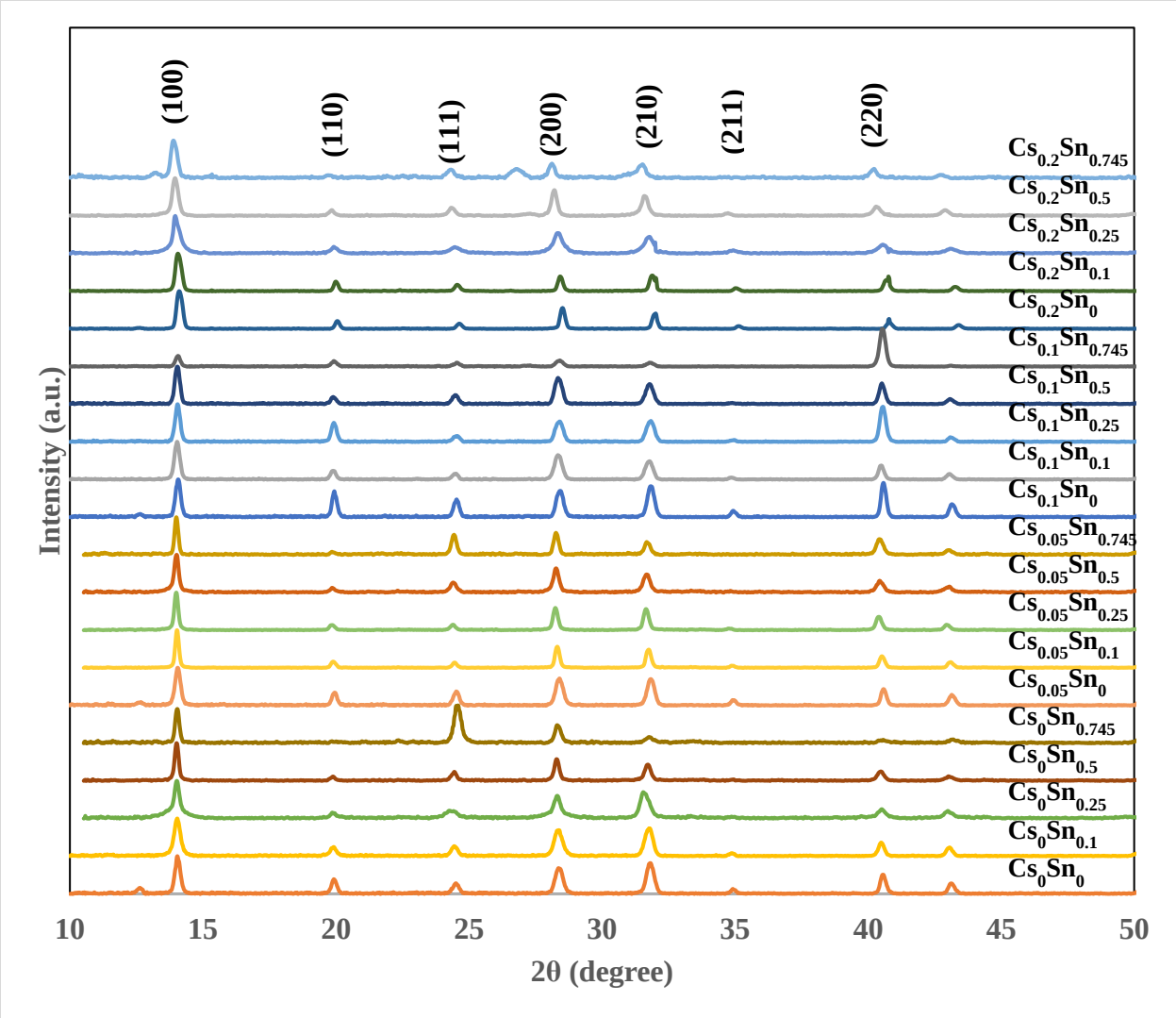

Figure 3. 37. XRD patterns of $Cs_x(MA_{0.17}FA_{0.83})_{1-x}Pb_{1-y}Sn_y(I_{0.83}Br_{0.17})_3$ perovskite thin films fabricated with a total precursor concentration of 2.5 M (no SnF_2) and with100 µL chlorobenzene anti-solvent.

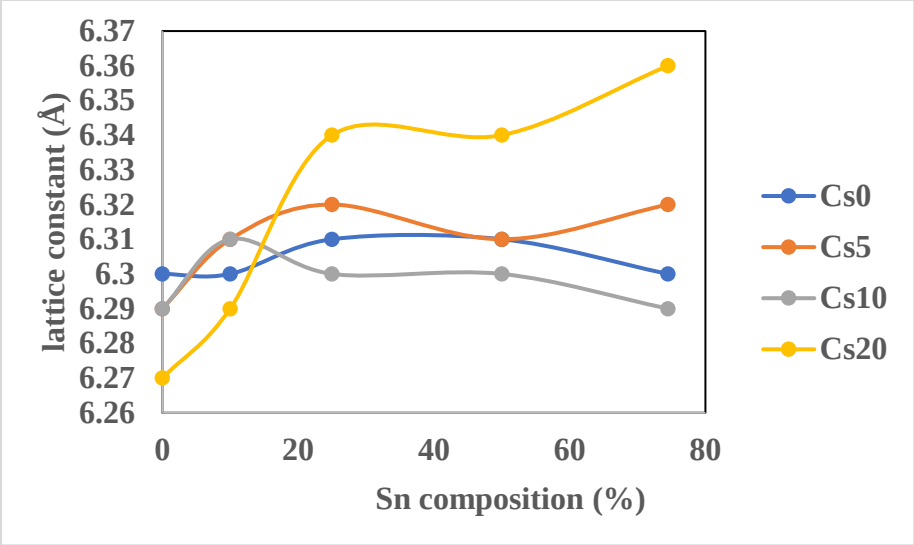

Figure 3. 38. Lattice constant of perovskite thin films as a function of Sn composition for 0, 5, 10 and 20% Cs determined from X-ray diffraction pattern.

The thin films were characterized by XRD to determine the phase and crystallinity. For Cs_0, there are two side peaks before 14˚, which correspond to the δ-$FAPbI_3$ and cubic PbI_2. They disappeared as more Cs and Sn were added. Adding Cs to the FA/MA cation decreases the average of cation radius since Cs has a much smaller ionic radius (r = 1.67 Å) which would also decrease the d-spacing according to Bragg's Law. Therefore, when keeping Sn constant at 0 %, by increasing Cs, there is a right shift in 2 θ. The increase of Cs also shifts the tolerance factor towards a cubic lattice structure that matches the black perovskite cubic phase [4]. The introduction of Cs removes contamination peaks, and Sn prevents phase change. However, according to the Bragg's law, the lattice constant, calculated from the (100) peak in Figure 3.37, should decrease as the increase of Cs composition. This trend was not shown in Figure 3.38, which could be due to the phase segregation of the perovskite thin films observed in photographs (Table 6) and the oxidation of the SnI_2 stock solution which cause the solution to be red instead of yellow.

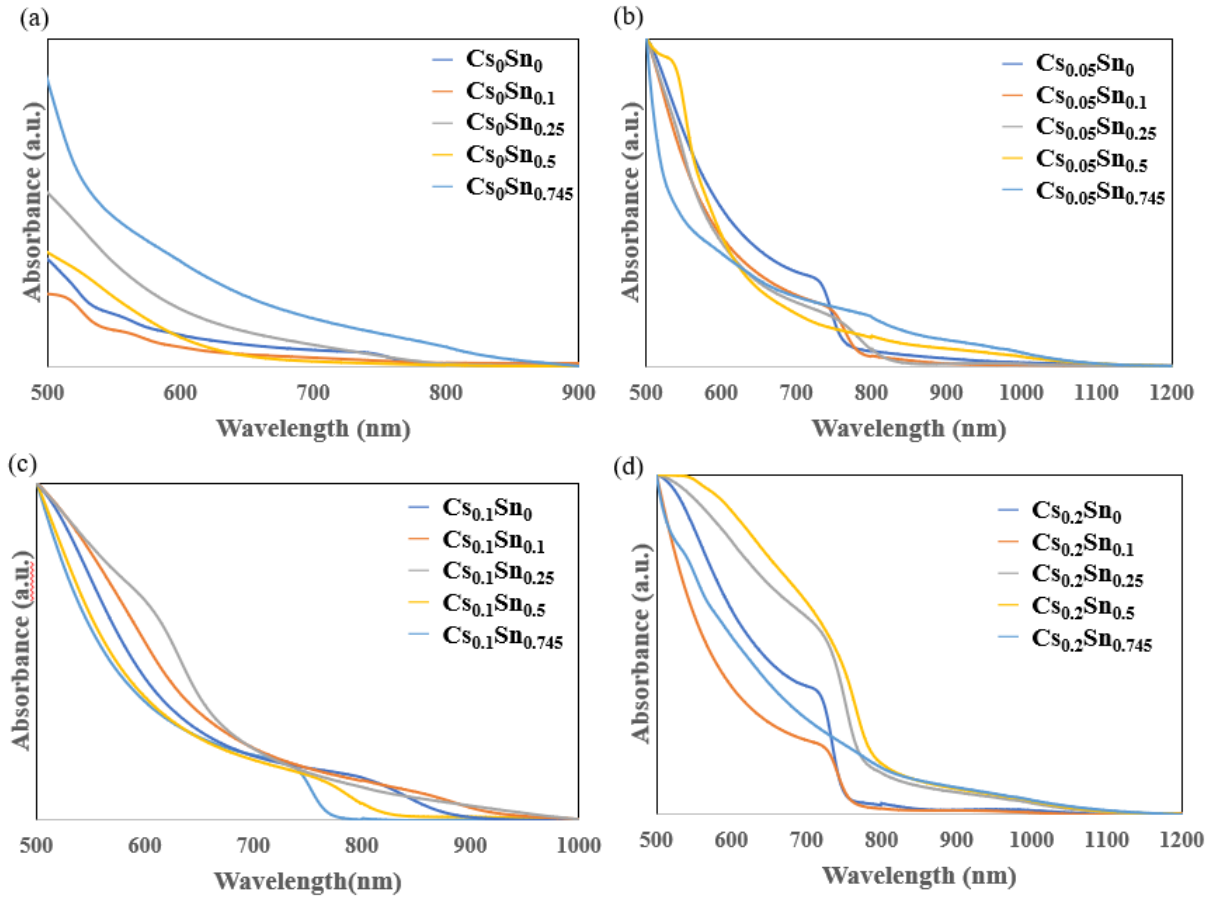

Figure 3. 39. UV-Vis spectra of $Cs_x(MA_{0.17}FA_{0.83})_{1-x}Pb_{1-y}Sn_y(I_{0.83}Br_{0.17})_3$ perovskite thin films with a total concentration of 2.5 M, with (a) x = 0, (b) x = 0.05, (c) x = 0.1 and (d) x = 0.2 and y = 0, 0.1, 0.25, 0.5 and 0.745, respectively, with 100 µL chlorobenzene anti-solvent.

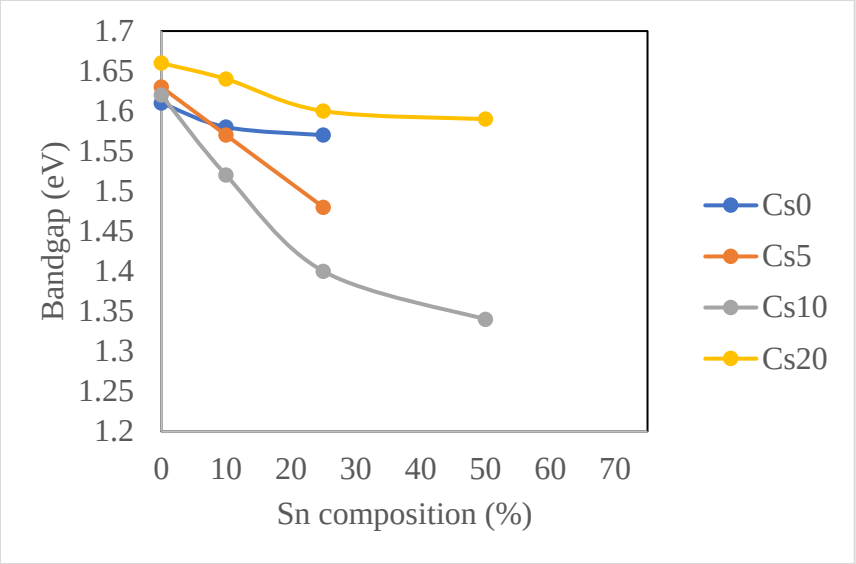

Figure 3. 40. Bandgap of perovskite thin films as a function of Sn composition for 0, 5, 10 and 20% Cs determined from UV-Vis absorption spectra.

The perovskite thin films displayed a broad absorbance toward the near-infrared region. As shown in Figure 3.39, with the increase of Cs in the perovskite films, the UV- Vis absorption edge blue shifts slightly, decreasing the bandgap. As Tin in the perovskite composition increased from 0 to 0.745, the absorption edge has a significant red shift. The band edge softens as the tin composition increases from 10 % to 25 % due to the existence of sub-bandgap states and the increase of scattering. The bandgaps were estimated from the band edges observed in the UV-Vis spectra in Figure 3.39 and plotted as a function of Sn composition shown in Figure 3.40. However, the bandgaps of the films with 74.5% Sn were not able to obtain due to the soften band edges and the low upper limit setting in acquiring the UV- Vis spectra.

3.3 Perovskite Thin Films Fabricated with Mixed Solvent of DMF and DMSO with Toluene Anti-Solvent

It was reported that toluene was typically used as an anti-solvent for making Sn-based perovskite films [2]. Therefore, we fabricated Pb-Sn perovskite films with DMF:DMSO (4;1, v/v)

co-solvent [4] and using 700 µL toluene anti-solvent in the wash step. The spin conditions were the same [2].

Table 7. The photographs of fresh $Cs_x(MA_{0.17}FA_{0.83})_{1-x}Pb_{1-y}Sn_y(I_{0.83}Br_{0.17})_3$ perovskite thin films with a total concentration of 2.5 M (no SnF_2) and with 700 µL toluene anti-solvent.

	Sn_0	**$Sn_{0.1}$**	**$Sn_{0.25}$**	**$Sn_{0.5}$**	**$Sn_{0.745}$**
Cs_0		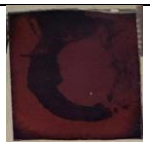			
$Cs_{0.05}$		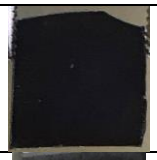			
$Cs_{0.1}$	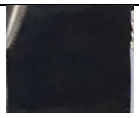				
$Cs_{0.2}$			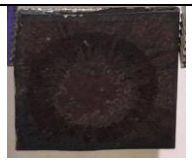		

Comparing Table 6 and Table 7, the change of anti-solvent from chlorobenzene to toluene resulted in the films retaining darker brown color for high Sn compositions, despite even more obvious segregations. When increasing Sn composition from 10% to 25 %, the grain boundaries smeared with more pinholes but grain size increased (Figure 3.41).

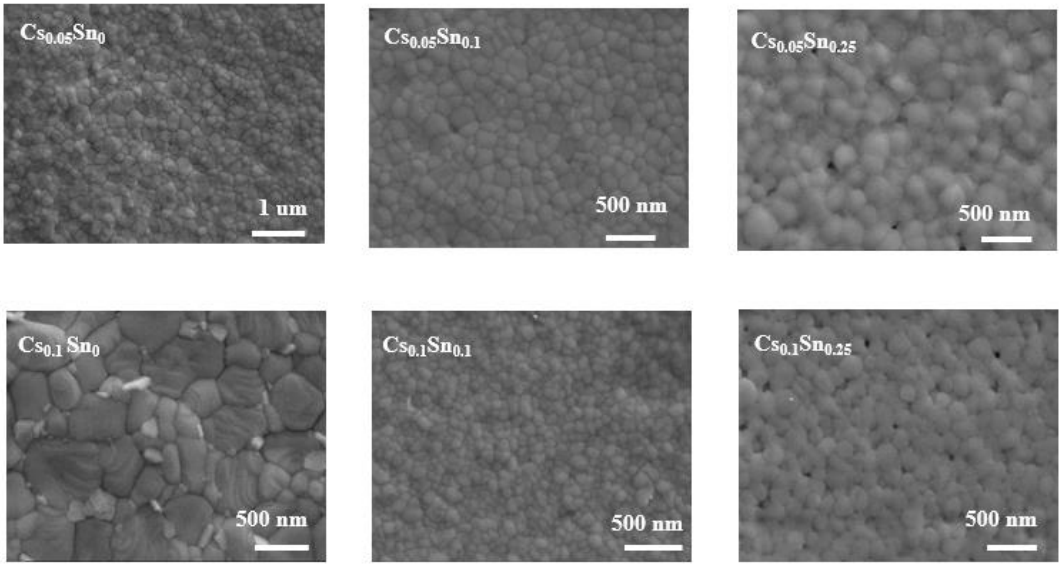

Figure 3. 41. SEM images of $Cs_x(MA_{0.17}FA_{0.83})_{1-x}Pb_{1-y}Sn_y(I_{0.83}Br_{0.17})_3$ perovskite thin films fabricated with a total precursor concentration of 2.5 M (no SnF_2) and with 700 µL toluene anti-solvent.

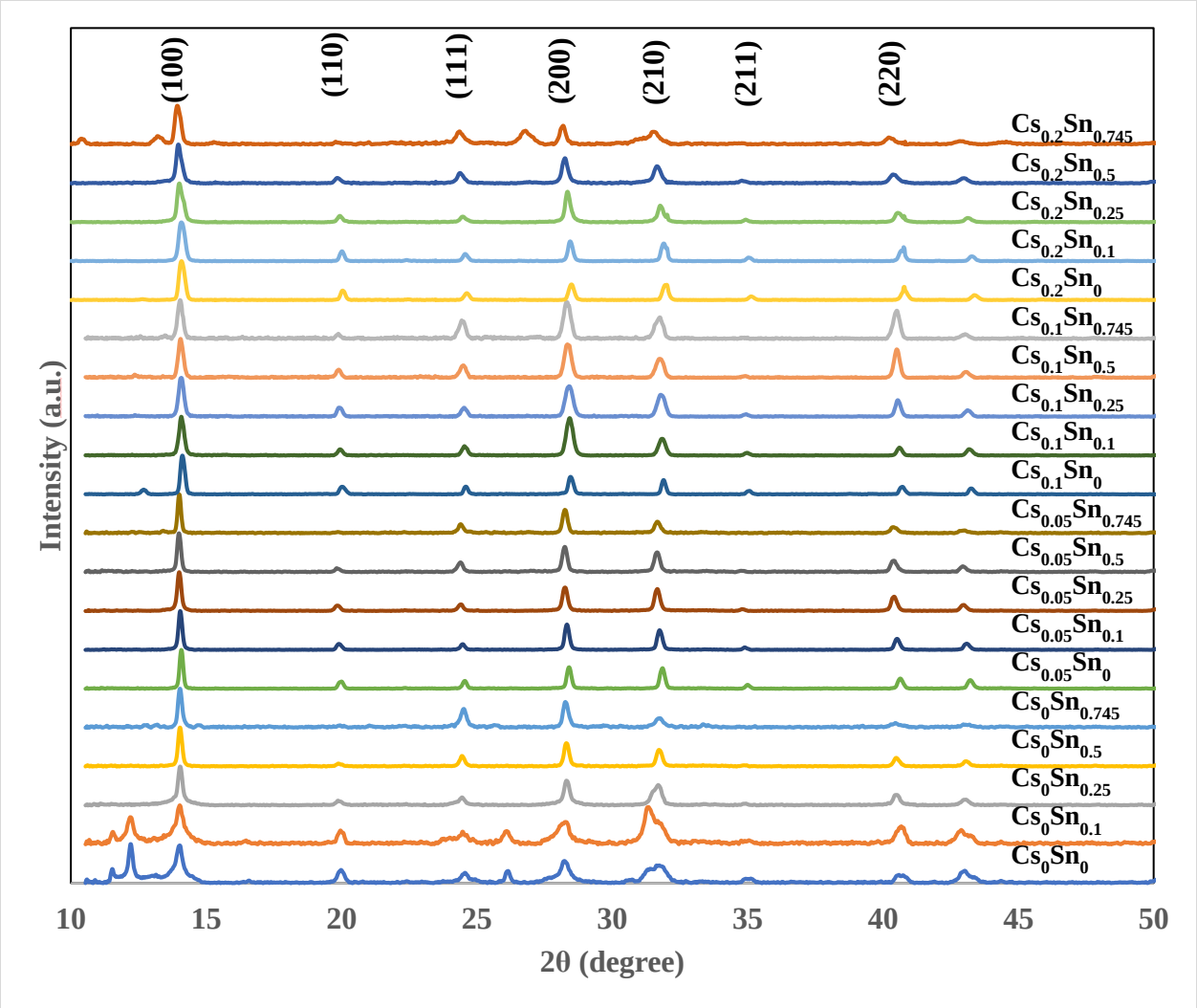

Figure 3. 42. XRD patterns of $Cs_x(MA_{0.17}FA_{0.83})_{1-x}Pb_{1-y}Sn_y(I_{0.83}Br_{0.17})_3$ perovskite thin films fabricated with a total precursor concentration of 2.5 M (no SnF_2) and with 700 µL toluene anti-solvent.

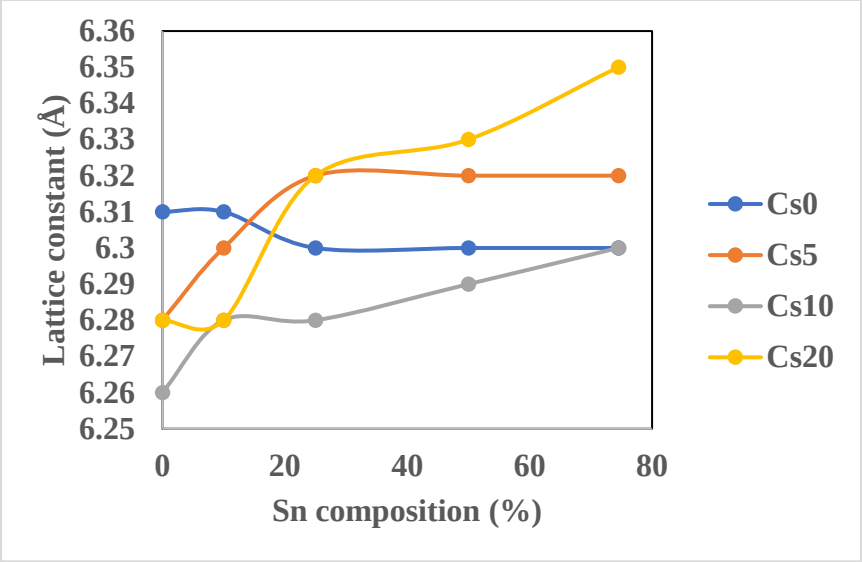

Figure 3. 43. Lattice constant of the (100) plane of perovskite thin films as a function of Sn composition for 0, 5, 10 and 20% Cs determined from X-ray diffraction patterns.

The XRD results (Figure 3.42) show that for Cs_0 films, there are two side peaks before 14˚, which correspond to the δ-$FAPbI_3$ and cubic PbI_2. They disappeared as more Cs and tin were added. Similarly, (110) and (211) peaks became weak and even disappeared when Sn composition was increased to 74.5%. In theory, as the increase of Cs, the lattice constant should decrease. However, the lattice constants of $Cs_{0.2}$ films were larger than those of $Cs_{0.05}$ films (Figure 3.43) especially when tin composition was increased. This could be due to the phase segregation of the film (Table 7) and the oxidation of the SnI_2 stock solution which cause the solution to be red instead of yellow.

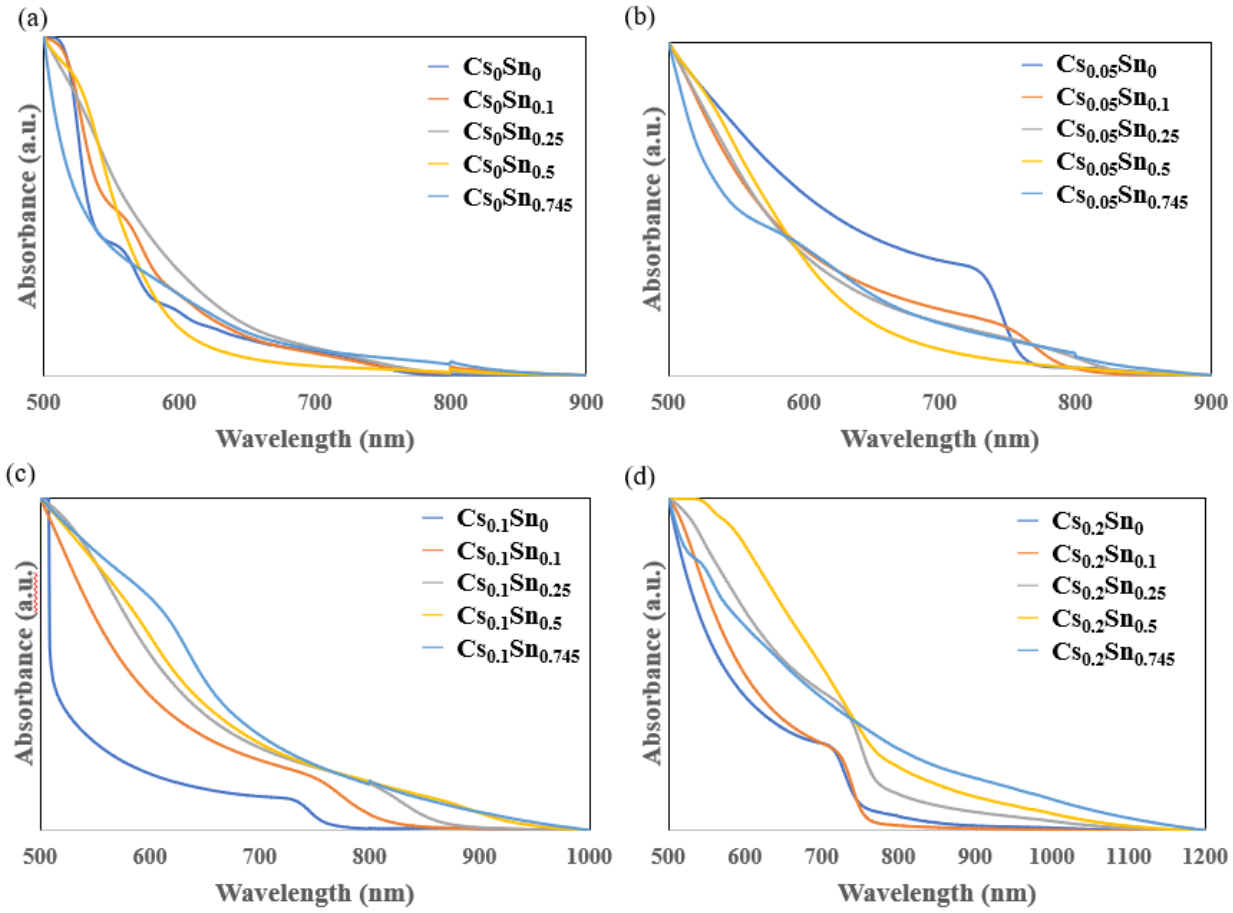

Figure 3. 44. UV-Vis spectra of $Cs_x(MA_{0.17}FA_{0.83})_{1-x}Pb_{1-y}Sn_y(I_{0.83}Br_{0.17})_3$ perovskite thin films fabricated with a total precursor concentration of 2.5 M (no SnF_2) and with 700 µL toluene anti-solvent.

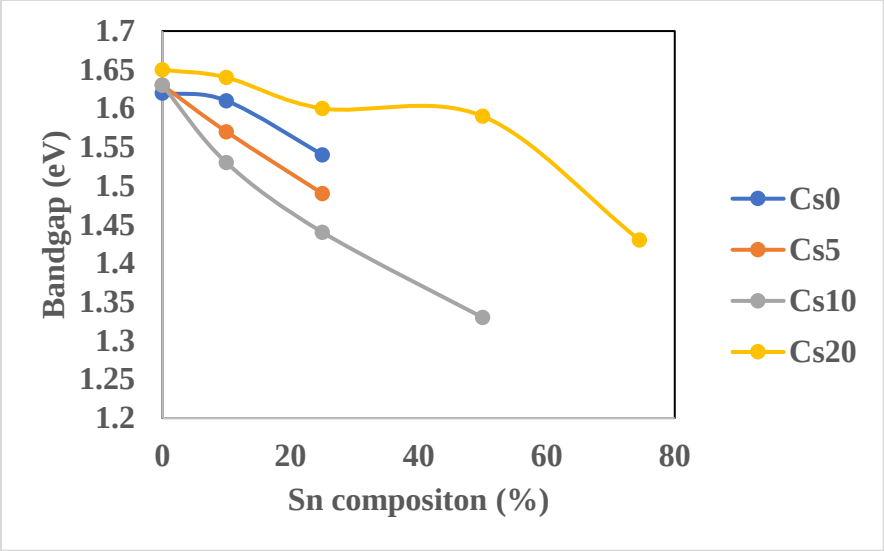

Figure 3. 45. Bandgap of perovskite thin films as a function of Sn composition for 0, 5, 10 and 20% Cs determined from UV-Vis absorption spectra.

The UV-Vis spectra (Figure 3.44) show that the increase of Cs in the perovskite films induced a slight blue shift of absorption edge, the estimated bandgaps of the perovskite thin films were plotted as a function of Sn composition for different Cs contents (Figure 3.45). It clearly shows the decrease of bandgap with the increase of Sn. However, the trend for Cs is not consistent.

According to Figure 3.43 and Figure 3.15, with the change of co-solvent from DMF: DMSO (4:1, v/v) to GBL: DMSO (7:3, v/v), lattice constants became smaller so did bandgaps by comparing Figure 3.45 and Figure 3.13.

Since the GBL: DMSO co-solvent was used for making Pb-Sn binary perovskites [2] and DMF: DMSO co-solvent was typically used for making Cs/MA/FA triple cation perovskites [4], we hypothesized a triple co-solvent of GBL, DMF and DMSO could be an option for making $Cs_x(MA_{0.17}FA_{0.83})_{1-x}Pb_{1-y}Sn_y(I_{0.83}Br_{0.17})_3$ perovskites. We made perovskite precursor solutions

with a total concentration of 2.5 M (no SnF_2) and with triple co-solvents in different ratios, GBL: DMF: DMSO (v/v/v) = 1:7:2, 2:6:2, 3:5:2, 4:4:2 and 5:3:2.

Table 8. The photographs of fresh $Cs_{0.05}(MA_{0.17}FA_{0.83})_{0.95}Pb_{0.9}Sn_{0.1}(I_{0.83}Br_{0.17})_3$ perovskite thin films fabricated with triple co-solvents (no SnF_2) and with 700 µL toluene anti-solvent.

GBL: DMF: DMSO	1:7:2	2:6:2	3:5:2	4:4:2	5:3:2
			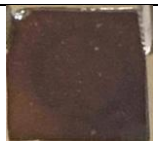		

All precursor solutions led to uniform dark brown color films as shown in Table 8. Figure 3.46 shows the grain size increased as GBL increases in the ratio of the co-solvent for making perovskite precursor solutions. The grains also have clear boundaries. The films fabricated with different ratios of triple co-solvent precursor solution resulted similar UV- Vis spectra and XRD patterns, shown in Figure 3.47 and 3.48, respectively, which indicate that the ratios of the three solvents won't affect the optical and crystalline properties.

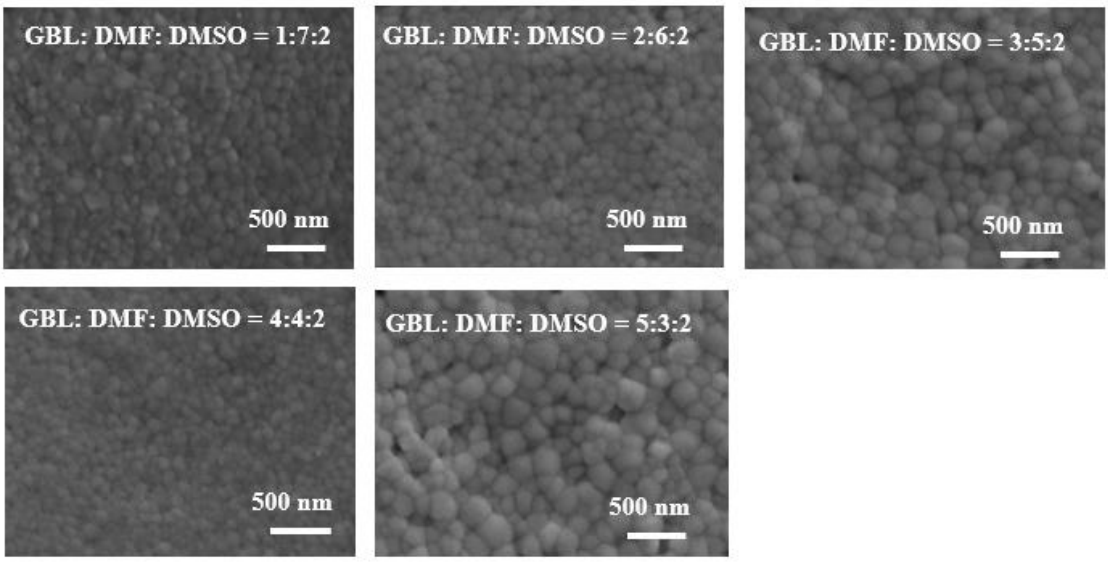

Figure 3. 46. SEM images of $Cs_{0.05}(MA_{0.17}FA_{0.83})_{0.95}Pb_{0.9}Sn_{0.1}(I_{0.83}Br_{0.17})_3$ perovskite thin films fabricated with total precursor concentration of 2.5 M (no SnF_2) solutions in different ratios of triple co-solvents and with 700 µL toluene anti-solvent.

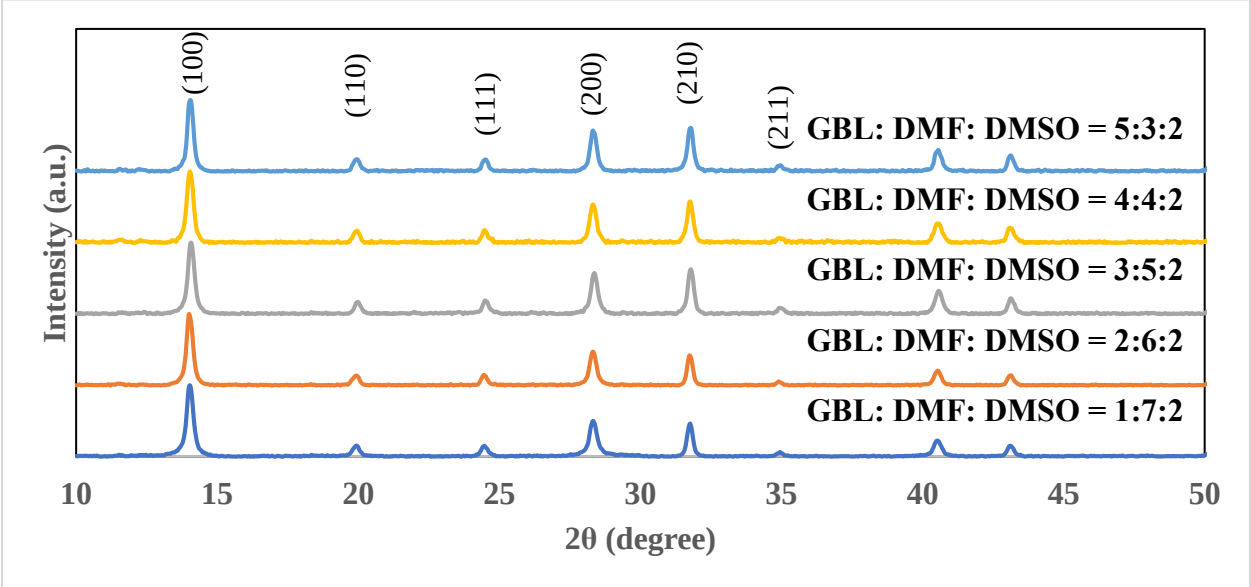

Figure 3. 47. XRD patterns of $Cs_{0.05}(MA_{0.17}FA_{0.83})_{0.95}Pb_{0.9}Sn_{0.1}(I_{0.83}Br_{0.17})_3$ perovskite thin films with a total concentration of 2.5 M (no SnF_2) using different ratio of solvent mixtures and with 700 µL toluene anti-solvent.

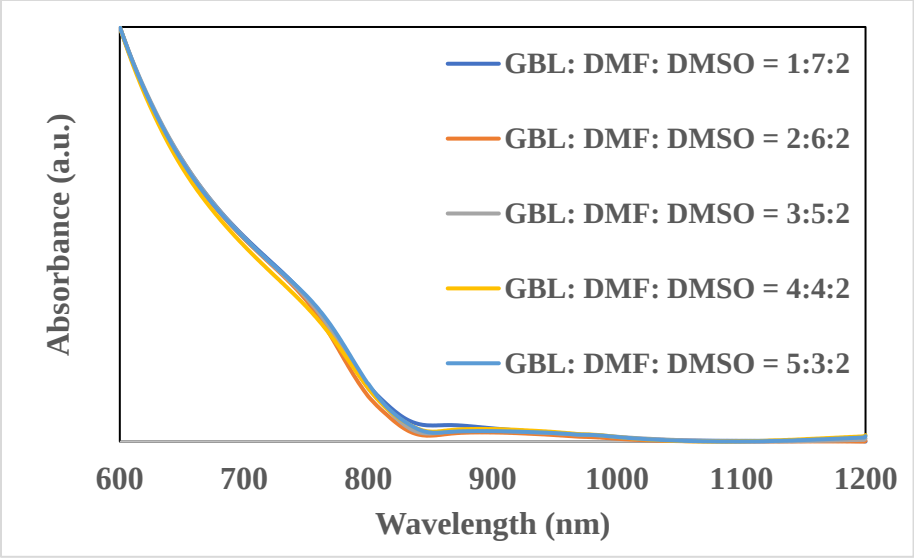

Figure 3. 48. UV-Vis spectra of $Cs_{0.05}(MA_{0.17}FA_{0.83})_{0.95}Pb_{0.9}Sn_{0.1}(I_{0.83}Br_{0.17})_3$ perovskite thin films with a total concentration of 2.5 M (no SnF_2) using different ratio of solvent mixtures and with 700 µL toluene anti-solvent.

Chapter 4 – CONCLUSIONS

This work focused on the optimization of morphological, crystalline and electronic properties of triple organic-inorganic cation Cs/FA/MA binary metal cation Pb/Sn and double halide Br/I perovskites thin films through the use of different co-solvents, anti-solvents, annealing conditions and addition of reducing agent in the fabrication of these perovskite films. The ambient air stability of the perovskite thin films was also assessed. It was found that the addition of SnF_2 in the precursor solution, the use of GBL:DMSO co-solvent and toluene anti-solvent are critical to achieve high quality $Cs_x(MA_{0.17}FA_{0.83})_{1-x}Pb_{1-y}Sn_y(I_{0.83}Br_{0.17})_3$ films. To produce pinhole-free, dense pure Sn perovskite thin films, the annealing conditions and the volume of toluene anti-solvent both need to be optimized.

REFERENCES

1. L. Zhu *et al.*, “Solvent-molecule-mediated manipulation of crystalline grains for efficient planar binary lead and tin triiodide perovskite solar cells”, *Nanoscale*, 2016, 8, 7621.
2. Z. Yang *et al.*, “Stable Low-Bandgap Pb-Sn Binary Perovskites for Tandem Solar Cells”, *Adv. Mater.*, 2016, 28, 8990-8997.
3. D. Bi *et al.*, “Efficient luminescent solar cells based on tailored mixed-cation perovskties”, *Sci. Adv.*, 2016, 2, e 1501170.
4. M. Saliba *et al.*, “Cesium-containing triple cation perovskite solar cells: improved stability, reproducibility and high efficiency”, *Energy Environ. Sci.*, 2016, 9, 1989-1997.
5. Z. Yang *et al.*, “Effect of formamidinium and bromide ion substitution in methylammonium lead triiodide toward high -performance perovskite solar cells”, *Nano Energy*, 2016, 22, 328 -337.
6. H. Tan *et al.*, “Efficient and stable solution-processed planar perovskite solar cells via contact passivation”, *Science* 355, 2017, 722 -726.
7. NREL Efficiency chart, https://www.nrel.gov/pv/assets/images/efficiency-chart.png).
8. M. Lee *et al.*, “Efficient Hybrid Solar Cells Based on Meso -Superstructured Organometal Halide Perovskties”, *Science*, 2012, 338 (6107), 643 -647.
9. T. M. Koh *et al.*, “Formamidinium-Containing Metal-Halide: An Alternative Material for Near-IR Absorption Perovskite Solar Cells,” *J. Phys. Chem. C*, vol. 118, pp. 16458–16462, Dec. 2013.
10. H.-S. Kim and N.-G. Park, “Lead Iodide Perovskite Sensitized All-Solid-State Submicron Thin Film Mesoscopic Solar Cell with Efficiency Exceeding 9%,” *Nature Scientific Reports*. pp. 1–7, 21-Aug-2012.

11. W. Liao *et al.*, “Lead-Free Inverted Planar Formamidinium Tin Triiodide Perovskite Solar Cells Achieving Power Conversion Efficiencies up to 6.22%,” *Adv. Mater.*, vol. 28, pp. 9333–9340, Aug. 2016.
12. J. H. Heo, D. H. Song, and S. H. Im, “Planar CH3NH3PbBr3Hybrid Solar Cells with 10.4% Power Conversion Efficiency, Fabricated by Controlled Crystallization in the Spin-Coating Process,” *Adv. Mater.*, vol. 26, pp. 8179–8183, Oct. 2014.
13. P. Prajongtat and T. Dittrich, “Precipitation of CH3NH3PbCl3 in CH3NH3PbI3 and Its Impact on Modulated Charge Separation,” *J. Phys. Chem. C*, vol. 119, pp. 9926–9933, Apr. 2015.
14. J. Noh *et al.*, “Chemical Management for Colorful, Efficient, and Stable Inorganic-Organic Hybrid Nanostructured Solar Cells”, *Nano Lett.*, 13, 4, 1764 -1769.
15. B. Conings *et al.*, “Intrinsic Thermal Instability of Methylammonium Lead Trihalide Perovskite,” *Adv. Energy Mater.*, vol. 5, p. 1500477, Jun. 2015.
16. C. Stoumpos and M. Kanatzidis, “Semiconducting Tin and Lead Iodide Perovskites with Organic Cations: Phase Transitions, High Mobilities, and Near-Infrared Photoluminescent Propertieproperties.pdf,” *Inorganic Chemistry*, vol. 52. pp. 9019–9038, 08-Jul-2013.
17. R. K. Misra *et al.*, “Temperature- and Component-Dependent Degradation of Perovskite Photovoltaic Materials under Concentrated Sunlight,” *J. Phys. Chem. Lett.*, vol. 6, pp. 326–330.
18. T. Matsui *et al.*, “Room-Temperature Formation of Highly Crystalline Multication Perovskites for Efficient, Low-Cost Solar Cells”, *Adv. Mater.*, 2017, 29, 1606258.

19. J. Xi *et al.*, “Multichannel Interdiffusion Driven $FASnI_3$ Film Formation Using Aqueous Hybrid Salt/ Polymer Solutions toward Flexible Lead- Free Perovskite Solar Cells”, *Adv. Mater.*, 2017, 29, 10606964.
20. A. Yusoff *et al.*, “Ambipolar Triple Cation Perovskite Field Effect Transistors and Inverters”, *Adv. Mater.*, 2016, 1602940.
21. X. Liu *et al.*, “Improved efficiency and stability of Pb–Sn binary perovskite solar cells by Cs substitution,” *J. Mater. Chem.*, vol. 4, pp. 17939–17945, 2015.
22. A. G. Kontos *et al.*, “Structural Stability, Vibrational Properties, and Photoluminescence in CsSnI3 Perovskite upon the Addition of SnF2,” *Inorg. Chem.*, vol. 56, pp. 84–91, Dec. 2016.
23. I. Chung and M. Kanatzidis, “All-solid-state dye-sensitized solar cells with high efficiency,” *Nature*, vol. 485. pp. 486–489, 24-May-2012.
24. N. Li *et al.*, “Enhanced Moisture Stability of Cesium- Containing Compositional Perovskites by a Feasible Interfacial Engineering”, *Adv. Mater. Interfaces*, 2017, 4, 1700598.
25. B. Saparov and D. B. Mitzi, “Organic–Inorganic Perovskites: Structural Versatility for Functional Materials Design,” *Chem. Rev.*, vol. 116, pp. 4558–4596, Apr. 2016.
26. F. Zuo *et al.*, “Binary -Metal Perovskites Toward High-Performance Planar-Heterojunction Hybrid Solar Cells”, *Adv. Mater.*, 2014, 26, 6454-6460.
27. S. J. Lee *et al.*, “Fabrication of Efficient Formamidinium Tin Iodide Perovskite Solar Cells through SnF2–Pyrazine Complex,” *J. Am. Chem. Soc.*, vol. 138, pp. 3974–3977, Mar. 2016.
28. G. Eperon, L. Herz, and H. Snaith, “Formamidnium lead trihalide a broadly tunable perovskite for efficient planar heterojunction solar cells,” *Energy Environment Science*, vol. 7. pp. 982–988, 03-Jan-2014.

29. J.-W. Lee, D.-J. Seol, A.-N. Cho, and N.-G. Park, “High-Efficiency Perovskite Solar Cells Based on the Black Polymorph of HC(NH2)2PbI3,” *Adv. Mater.*, vol. 26, pp. 4991–4998, Jun. 2014.
30. N. J. Jeon *et al.*, “Compositional engineering of perovskite materials for high-performance solar cells,” *Nature*, vol. 517, pp. 476–480, Jan. 2015.
31. Z. Yang *et al.*, “Stabilized Wide Bandgap Perovskite Solar Cells by Tin Substitution”, *Nano Lett.*, 2016, 16, 7739-7747.